N77-17560

OPTIMIZATION OF ABSORPTION AIR-CONDITIONING FOR SOLAR ENERGY APPLICATIONS

Edward H. Perry

Memphis State University
Memphis, Tennessee

December 1976

OPTIMIZATION OF ABSORPTION AIR-CONDITIONING

FOR SOLAR ENERGY APPLICATIONS

FINAL REPORT

CONTRACT NAS8-31189

PREPARED FOR

NATIONAL AERONAUTICS AND SPACE ADMINISTRATION
GEORGE C. MARSHALL SPACE FLIGHT CENTER
HUNTSVILLE, ALABAMA

BY

MECHANICAL ENGINEERING DEPARTMENT
MEMPHIS STATE UNIVERSITY
MEMPHIS, TENNESSEE

DECEMBER 1976

OPTIMIZATION OF ABSORPTION AIR-CONDITIONING FOR SOLAR ENERGY APPLICATIONS

FINAL REPORT: CONTRACT NAS8-31189

PERFORMANCE PERIOD: 9-1-74 TO 10-31-76

PREPARED FOR

NATIONAL AERONAUTICS AND SPACE ADMINISTRATION
GEORGE C. MARSHALL SPACE FLIGHT CENTER
HUNTSVILLE, ALABAMA 35812

BY

EDWARD H. PERRY
MECHANICAL ENGINEERING DEPARTMENT
MEMPHIS STATE UNIVERSITY
MEMPHIS, TENNESSEE

DECEMBER 1976

SUMMARY

A study was undertaken to examine ways of improving the performance of solar cooling systems based on the lithium bromide-water absorption cycle. The study included computer simulations of a solar-cooled house, analyses and measurements of heat transfer rates in absorption system components, design and fabrication of various system components, and a brief survey of solar collector convection suppression methods.

TABLE OF CONTENTS

NOMENCLATURE

g	acceleration of gravity
$\bar{h}$	mean heat transfer coefficient
h_{fg}	heat of vaporization
h_x	local heat transfer coefficient
k	thermal conductivity
L	plate length
q	heat flux
T_{sat}	saturation temperature
T_w	plate temperature
v	fluid velocity parallel to plate
x	distance along plate
y	distance normal to plate
Γ	fluid mass flow rate per unit plate width
Γ_1	initial mass flow rate
δ	film thickness
δ_1	initial film thickness
θ	plate tilt angle
μ	dynamic viscosity coefficient
ρ	density
τ	shear stress

I. INTRODUCTION

It is estimated that space cooling accounts for approximately 4% of the energy used in the United States today {1}. Although this is a small fraction of the total energy consumption, it is the equivalent of 516 million barrels of crude oil annually and is, therefore, quite sizeable when viewed from a different perspective.

Solar cooling is a topic that has been explored considerably in the past. A number of studies have addressed the theoretical performance of various cooling systems {2 - 5}, projected economic benefits {6 - 8},and observed the actual operation of solar cooling systems {9 - 10}. For the most part these have fallen into one of two categories: (1) Rankine Cycle - Vapor Compression Cycle system; (2) Absorption Cycle System. Systems falling into the first category use heat derived from a solar energy collector to power a Rankine cycle engine, which typically used a flouro-carbon refrigerant such as R-114 as its working fluid. This Rankine cycle engine drives a conventional vapor compression cycle air-conditioner.

A typical absorption-cycle solar cooling system is shown schematically in Fig. 1-1. When cooling is needed, hot water from storage is pumped through the generator section of the absorption unit causing refrigerant vapor to be released from the solution present there. This refrigerant is subsequently condensed, evaporated, and re-absorbed by the solution. During

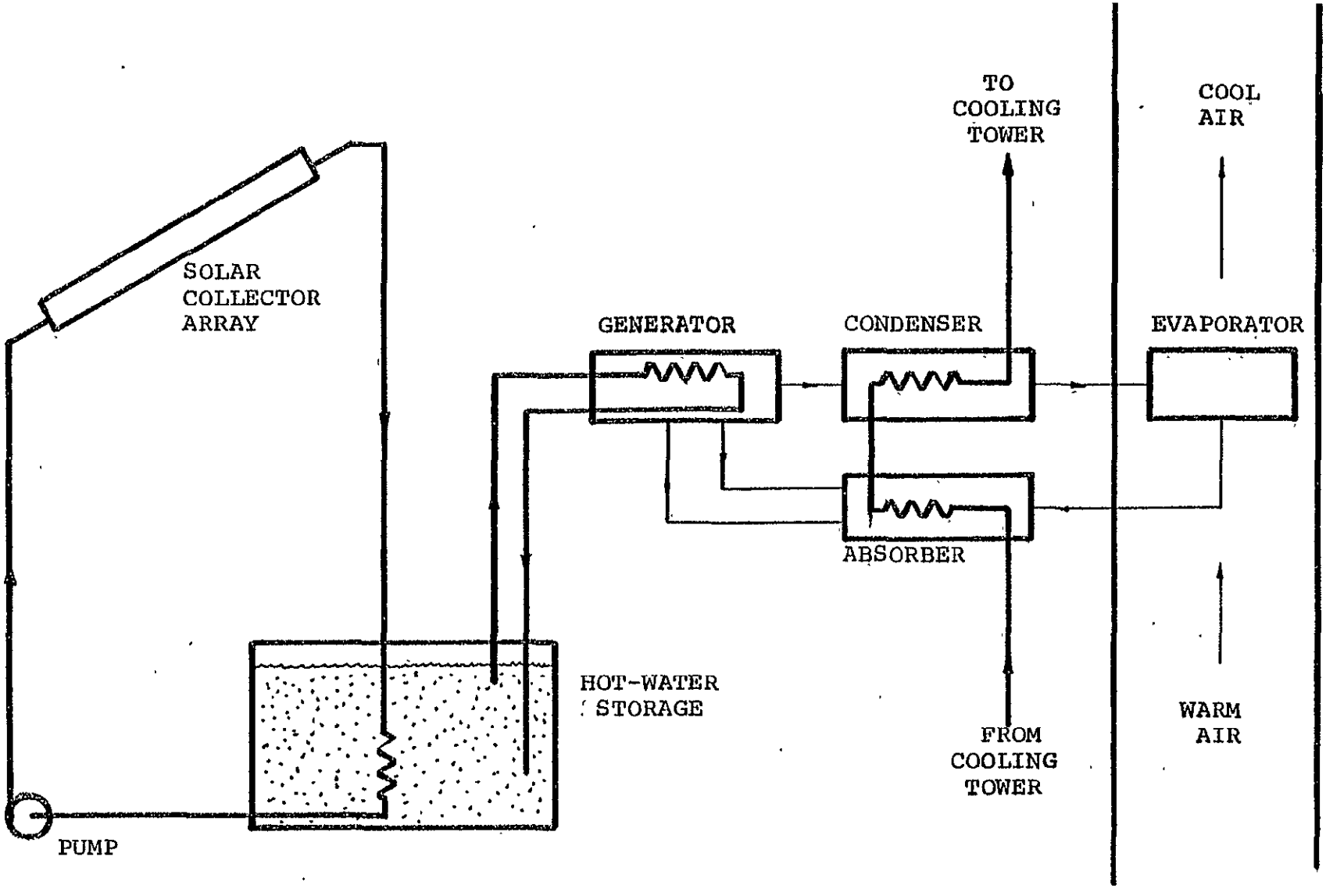

FIGURE 1-1. SCHEMATIC OF A TYPICAL SOLAR ENERGY-ABSORPTION COOLING SYSTEM.

these processes heat is given off to cooling water passing through the condenser and absorber, and heat is absorbed from the air passing over the evaporator coils. The latter process, of course, produces the desired solar cooling.

The present study was undertaken to examine ways of improving the performance of absorption cycle systems. In particular the lithium bromide-water absorption cycle was examined since it is the cycle used in existing solar cooling systems. The study included computer simulations of a solar cooled home, investigations of various heat transfer processes employed in absorption cycle equipment, and designs of several system components. Several results obtained during the study should improve the performance of future absorption cooling systems.

II. PERTINENT ASPECTS OF THE LITHIUM BROMIDE-WATER ABSORPTION COOLING PROCESS

In Fig. 2-1 a typical absorption-cycle cooling system is shown. During operation an aqueous solution of lithium bromide is pumped from the absorber to the generator where heat supplied by the solar collectors drives off water vapor, which becomes the refrigerant. The refrigerant is condensed and passed through a throttling valve, bringing about a decrease in both the pressure and temperature. In the evaporator the liquid refrigerant vaporizes by absorbing heat from the surroundings and thereby produces the desired cooling effect. This refrigerant vapor passes to the absorber where it is re-absorbed by the strong lithium bromide solution returning from the generator.

A typical thermodynamic process path for the cycle is shown in Fig. 2-2, where the system pressure is plotted versus the temperature. The numbers representing the various points around the cycle correspond to those points shown in Fig. 2-1. For example, state 1 represents the absorber exit state.

The equations representing the process are described in detail elsewhere {11-12} and will not be repeated here. Instead only those results pertinent to the present study will be discussed. In Fig. 2-3 the effects of cycle operating temperatures are shown. The coefficient of performance in all instances is defined as the ratio of the heat absorbed by the evaporator to that supplied the generator. For all cases shown no refrigerant pre-cooler was

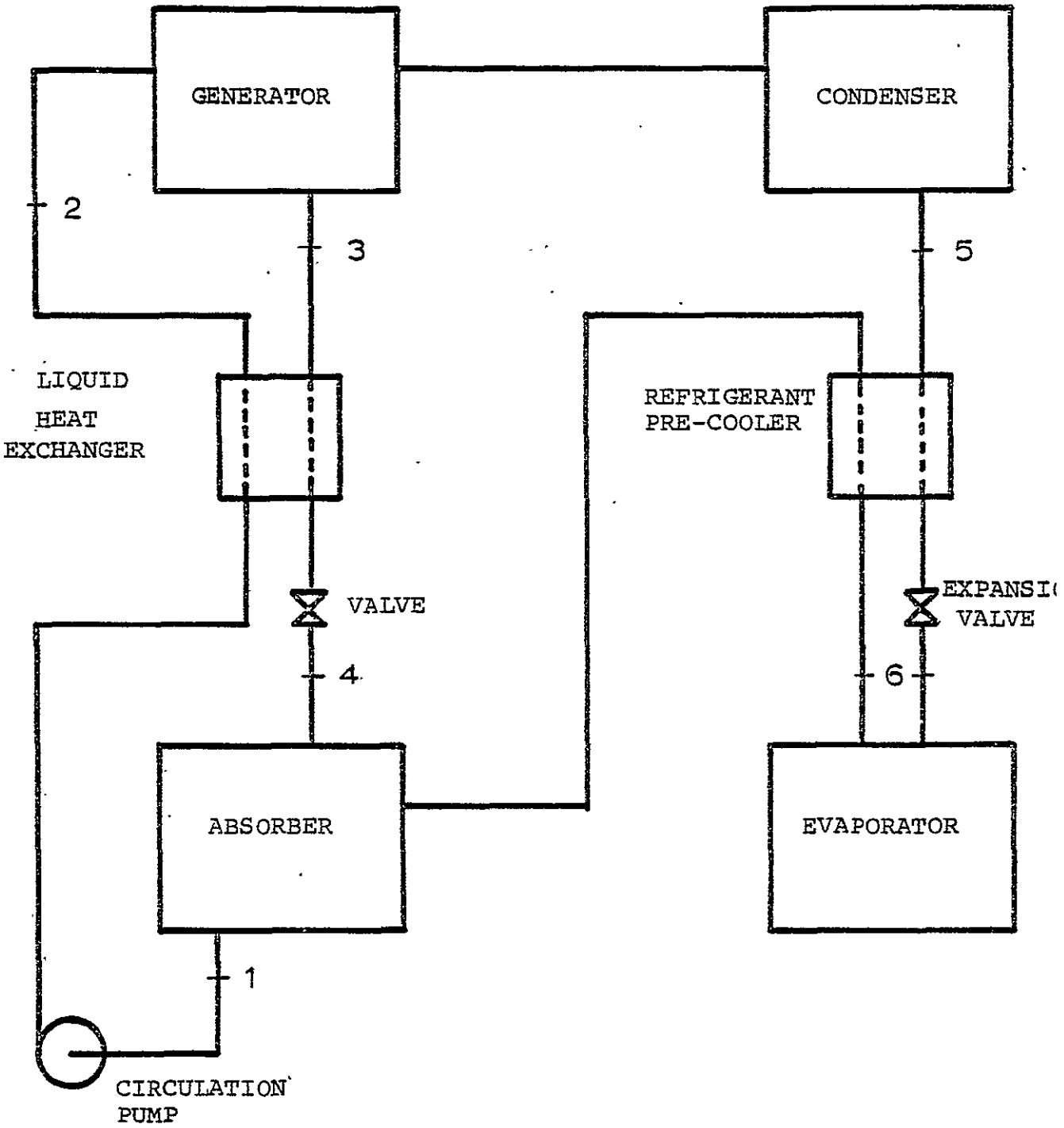

FIGURE 2-1. SCHEMATIC OF A TYPICAL ABSORPTION COOLING SYSTEM.

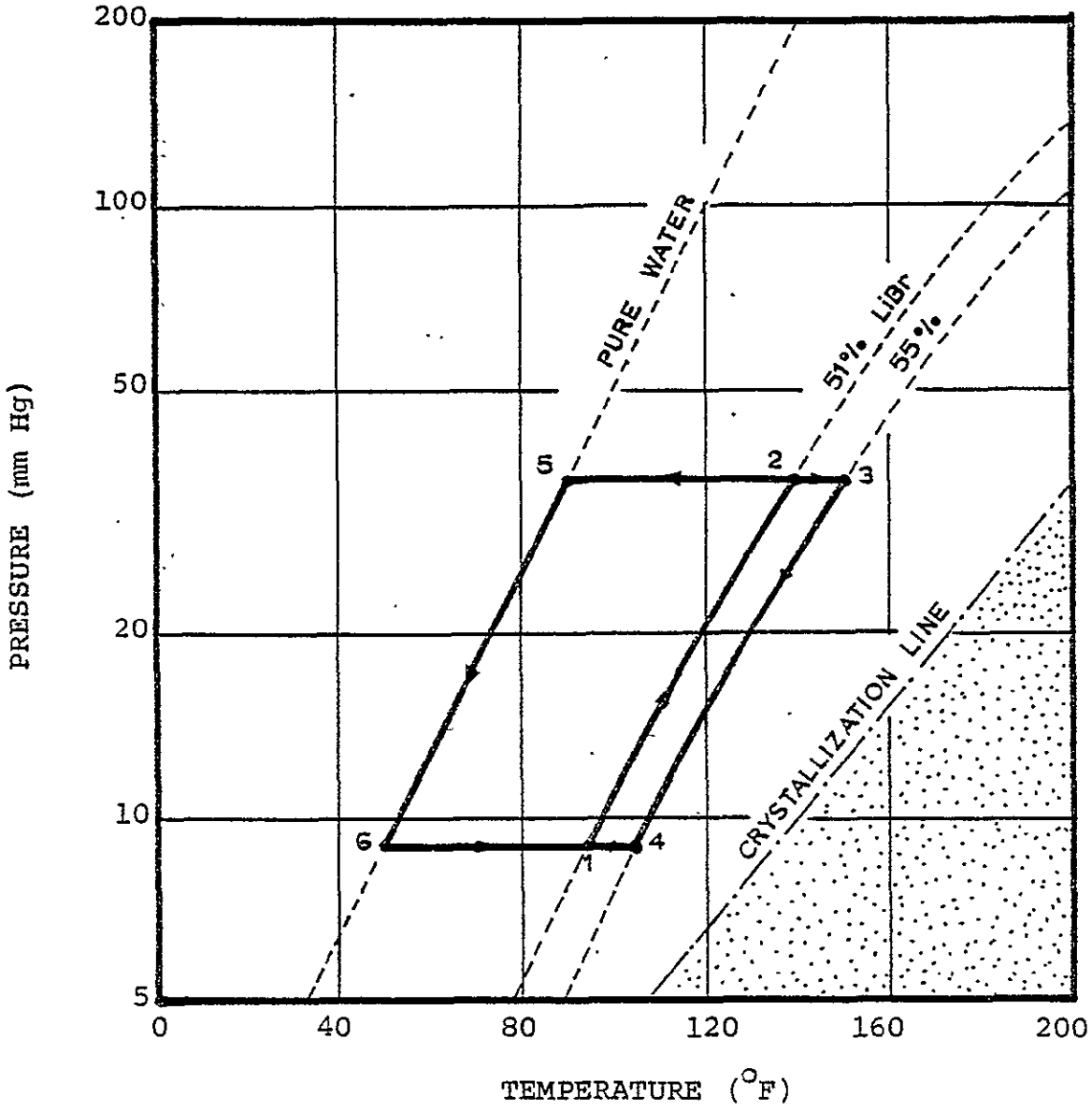

FIGURE 2-2..THERMODYNAMIC PATH OF A TYPICAL LITHIUM BROMIDE-WATER ABSORPTION CYCLE.

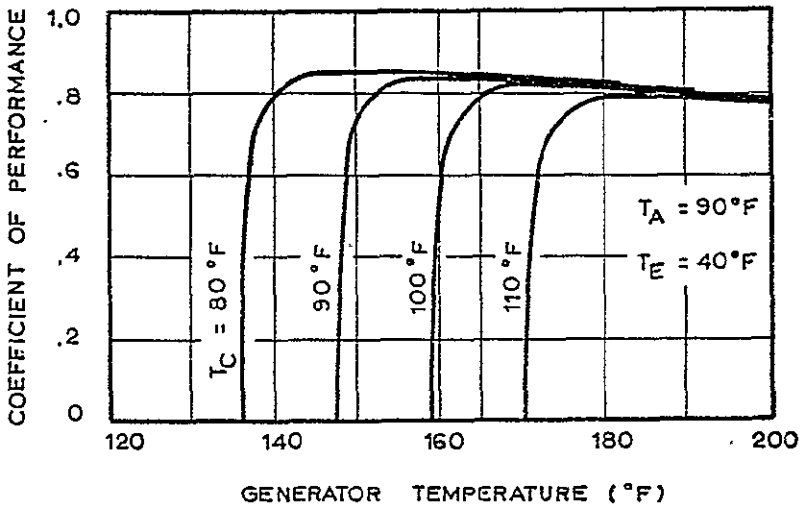

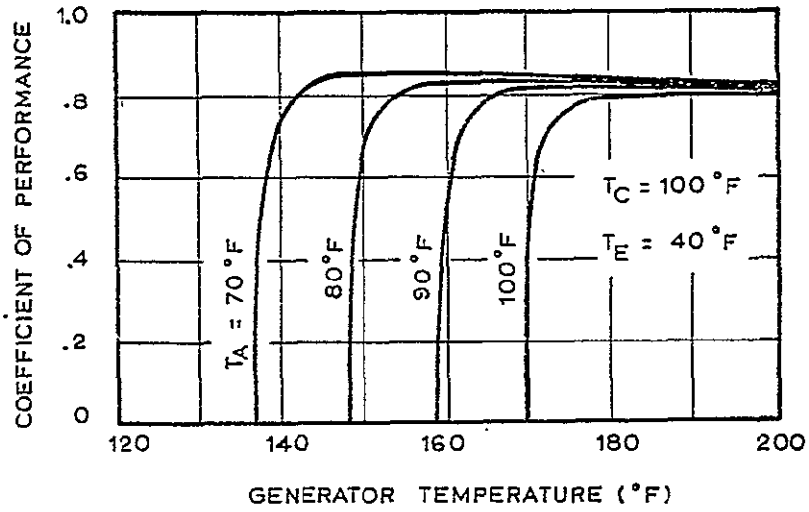

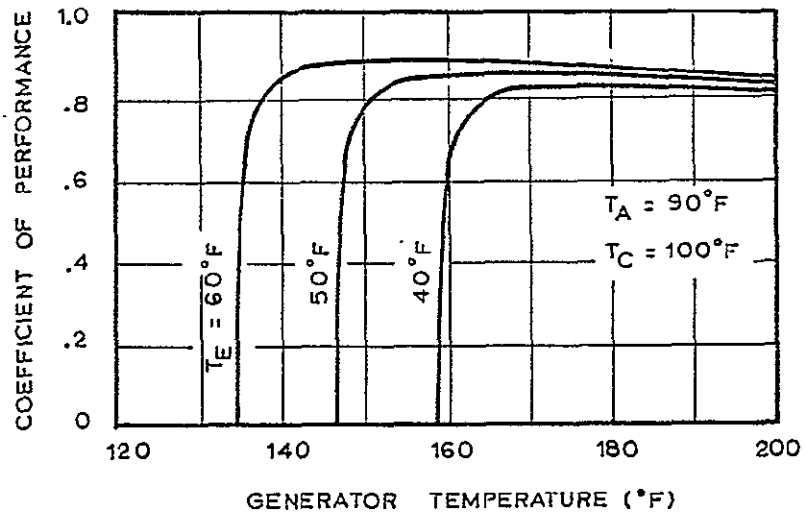

FIGURE 2-3. EFFECTS OF OPERATING TEMPERATURES ON THE COEFFICIENT OF PERFORMANCE.

taken to be present, and a liquid-liquid heat exchanger effectiveness of 0.9 was assumed.

Several important characteristics of the cycle are evident from Fig. 2-3. First, for given absorber, condenser, and evaporator temperatures no refrigeration occurs unless the generator is operated above a certain minimum or "cutoff" temperature. However, for generator temperatures above this cutoff value, the coefficient of performance rapidly increases to a maximum value and then slowly decreases with rising generator temperature. Physically the cutoff temperature corresponds to the saturation temperature of the solution entering the generator. Unless the generator temperature is above that value, no refrigerant vapor is driven from the solution, and no refrigeration occurs. In addition to a cutoff or minimum allowable generator temperature there is also a maximum allowable generator temperature which is due to crystal formation in the system. For some operating temperatures these maximum generator temperatures are below 200°F, and in such cases are represented by the terminations of the curves in Fig. 2-3.

Another characteristic observed in Fig. 2-3 is that for a particular generator temperature the coefficient of performance increases slightly as the condenser and absorber temperatures fall and as the evaporator temperature rises. This feature is best explained by viewing the absorption cycle as a heat engine driving a vapor compression refrigerator as discussed by Ellington et al. [11]. Since the engine rejects heat at the absorber temperature, the lower this value the higher the engine's efficiency. Similarly, the smaller the difference between the condenser

and evaporator temperatures, the greater the coefficient of performance of the vapor compression refrigerator. Since the coefficient of performance of the absorption cycle is simply the product of the engine's efficiency and the refrigerator's coefficient of performance, the behavior observed in Fig. 2-3 is to be expected.

An additional characteristic apparent from Fig. 2-3 is that the generator cutoff temperature increases with increasing condenser and absorber temperatures and decreasing evaporator temperature. This effect is shown more clearly in Fig. 2-4 where the cutoff temperature is given as a function of the condenser and absorber temperatures, which were assumed equal in this instance, for various evaporator temperatures. The behavior shown in Fig. 2-4 is due to the fact that the saturation temperature of the solution entering the generator increases with the solution concentration and the pressure within the generator.

High absorber temperatures and low evaporator temperatures result in high concentrations, and high condenser temperatures result in high generator pressures. Consequently, the observed effects are to be expected once again.

In summary, the coefficient of performance of the lithium bromide-water cooling cycle is relatively insensitive to changes in the cycle operating temperatures provided the generator temperature is above some minimum or cutoff temperature. This cutoff temperature does, however, depend on the other operating temperatures. From the standpoint of solar cooling optimization,

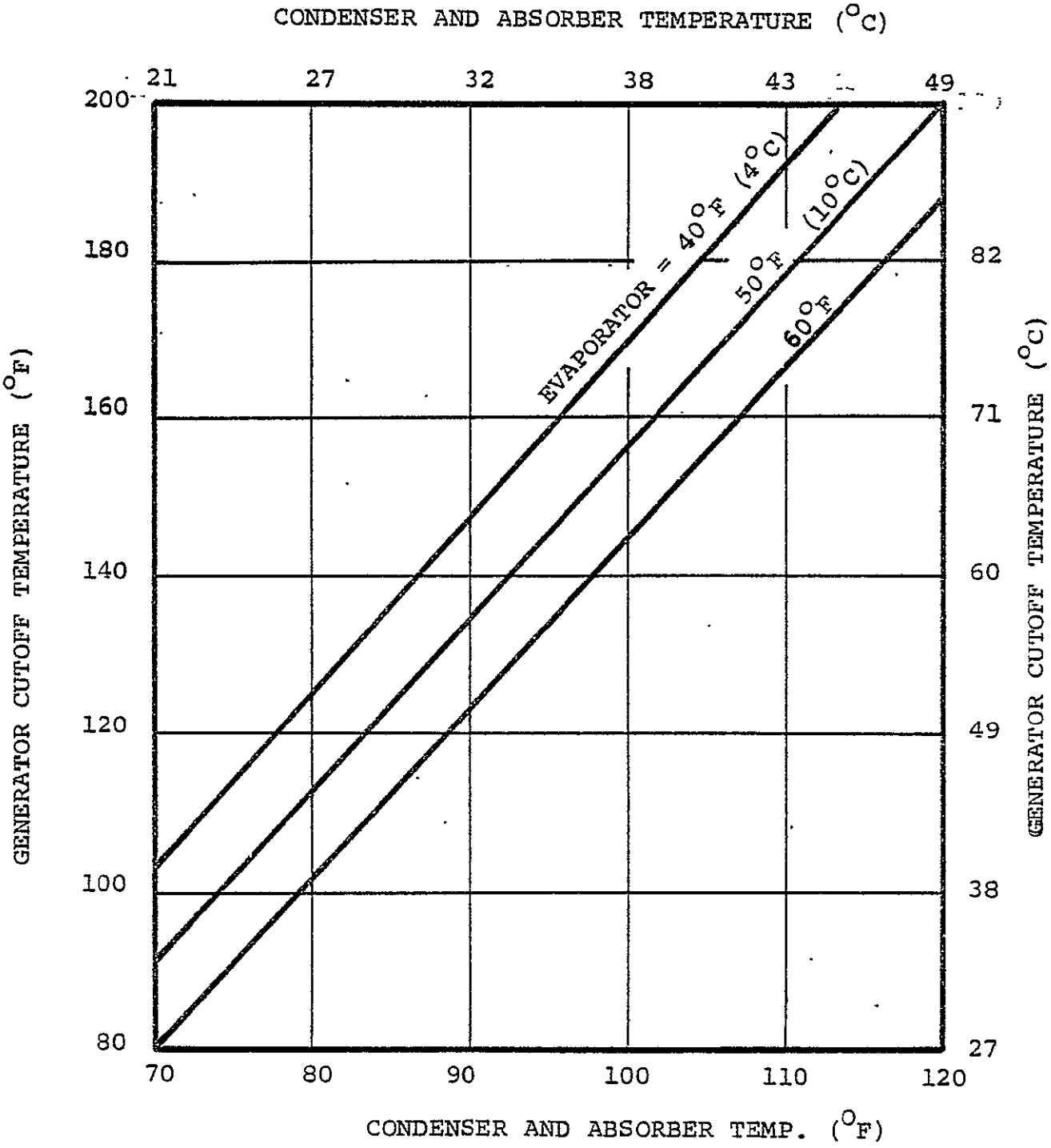

FIGURE 2-4. DEPENDENCE OF GENERATOR CUTOFF TEMPERATURE ON SYSTEM OPERATING TEMPERATURES.

every effort should be made to minimize this cutoff temperature since it is directly related to the solar collector operating temperature. Low condenser and absorber temperatures lead to low generator cutoff temperatures as does a high evaporator temperature.

III. SIMULATION STUDIES

In the normal, or daytime, mode of operation a solar absorption cooling system collects heat during the day via the solar collectors and produces cooling as it is needed (primarily during the day) via the absorption cooler. The only energy storage needed is the high-temperature storage normally associated with a solar collector array.

A second mode of operation is shown schematically in Fig. 3-1. During the day solar energy is collected and stored as before, but the absorption cooling unit remains idle until evening. At that time heat is taken from storage, cooling is produced by the absorption unit and stored for later use in a large tank of chill-water. The motivation behind this mode of operation is that it permits a lower condenser and absorber temperatures which, as was discussed earlier, permits lower generator and solar collector temperatures. Since solar collector efficiencies always decrease with increasing collector temperature, the nocturnal operation mode could exhibit improved performance over the conventional mode.

To determine the benefits, if any, derived from operating a solar absorption cooling system in this unconventional mode, computer simulations of a solar cooled house were carried out using first the conventional cooling mode and then the nocturnal cooling mode. Weather data similar to those prevailing in Memphis, Tennessee, were used in the simulations. Solar insolation in the collector plane was calculated assuming clear skies. A solar collector employing a non-selective absorber coating and two glass covers was also assumed.

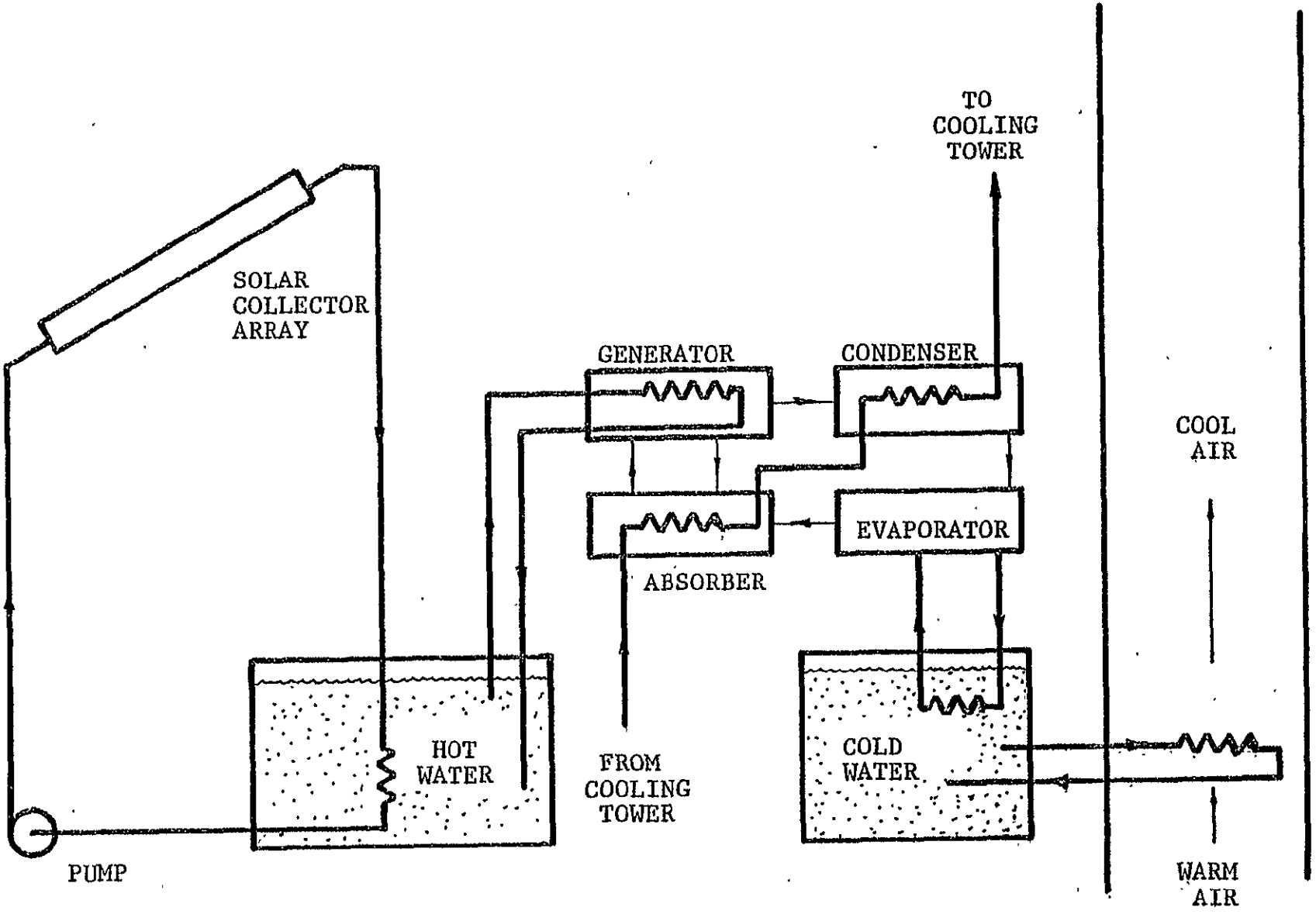

FIGURE 3-1. CONFIGURATION OF SYSTEM USED FOR NIGHTTIME MODE OF OPERATION.

A conventional 1500 FT^2 (139 M^2) home was used in all the simulations. A collector tilt angle equal to the local latitude (35° North) was selected, since presumably the collectors would also be used to supply space heat during the winter months. Cooling for the home was assumed to come from a 36,000 Btu/hr (10.6 kw) absorption unit which operates at constant capacity and with a coefficient of performance of 0.66 as long as the hot water supplied the generator remains at least 30°F (16.7°C) above the generator cutoff temperature. As discussed earlier, this cutoff temperature is very much dependent on the condenser, absorber, and evaporator temperatures.

It was assumed that the cooling water supplied in a series fashion to the condenser and absorber was 10°F (5.5°C) warmer that the prevailing wet-bulb temperature of the outside air during the period of operation. For the daytime operation mode a wet-bulb temperature of 78°F (25.6°C) was assumed, while for the nocturnal mode a value of 66°F (18.9°C) was assumed. These led to entering cooling water temperatures of 88°F (31.1°C) and 76°F (24.4°C), respectively. For both modes the absorber was assumed to operate at a temperature of 10°F (5.6°C) warmer than the entering cooling water and the condenser at a temperature 20°F (11.1°C) warmer than the entering cooling water. Thus the diurnal mode involved absorber and condenser temperatures of 98°F (36.7°C) and 108°F (42.2°C), respectively, while values of 86°F (30°C) and 96°F (35.6°C) were assumed for the nocturnal modes.

It was assumed that the cooling coils used to cool and de-humidify the air within the house operated at a temperature of 45°F (7.2°C). Since the diurnal mode involved a direct-expansion evaporator coil for this cooling coil, an evaporator temperature of 45°F (7.2°C) was assumed. Since the nocturnal mode involved an additional heat transfer process between the evaporator coil and the actual cooling coil, a lower evaporator temperature of 40°F (4.4°C) was assumed for this mode.

Using the operating temperatures described above a thermodynamic analysis of the lithium bromide-water absorption cycle was undertaken as described elsewhere {4}. This analysis revealed that a generator cutoff temperatures of 171°F (77.2°C) and 150°F (65.6°C) could be expected for the diurnal and nocturnal modes, respectively. Thus, entering hot-water temperatures of 201°F (93.9°C) and 180°F (82.2°C) respectively, were assumed for the two modes. Since the solar collector was assumed to operate at a temperature 10°F (5.5°C) warmer than the hot-water storage temperature, collector temperatures of 211°F (99°C) and 190°F (88°C) were assumed for the diurnal and nocturnal modes, respectively.

Simulations were performed for the 21st of each month from March through October. Since the purpose of the simulations was to compare the two modes of operation, the sky was presumed perfectly free of clouds. Thus, the results indicate the system performance for ideal sunny days. During each simulation each parameter was updated every 15 minutes and running totals of thermal energy used and solar energy collected were kept.

Fig. 3-2 presents results obtained for a typical simulation. Plotted as functions of time of day are the thermal load on the house, the solar energy collection rate, and the cooling supplied by the absorption air-conditioner. As expected, the thermal load and the collector output reach their maximum values at mid-afternoon and noon, respectively. For the day shown the collector array would be able to supply 100% of the energy required by the absorption unit.

Fig. 3-3 presents results which reveal one of the principle advantages of the nocturnal operational mode. The solar energy collection rate is plotted as a function of time of day for a sunny June 21st. The lower curve represents the collector performance associated with the day-time absorption cooling mode. The upper curve, displaying the characteristics of a collector operating at 190°F (88°C), represents the nighttime cooling mode. Two differences are readily apparent. First, the lower collector temperatures associated with the nighttime mode lead to higher instantaneous collection rates since the thermal losses to the environment are less. Second, lower collector temperatures permit longer collection periods, although this effect is generally of secondary importance. Combined, the two effects result in a 23% increase in the energy collected by the lower temperature collector. From a different perspective the nocturnal cooling mode would require 23% less collector area to provide the same amount of cooling on June 21st.

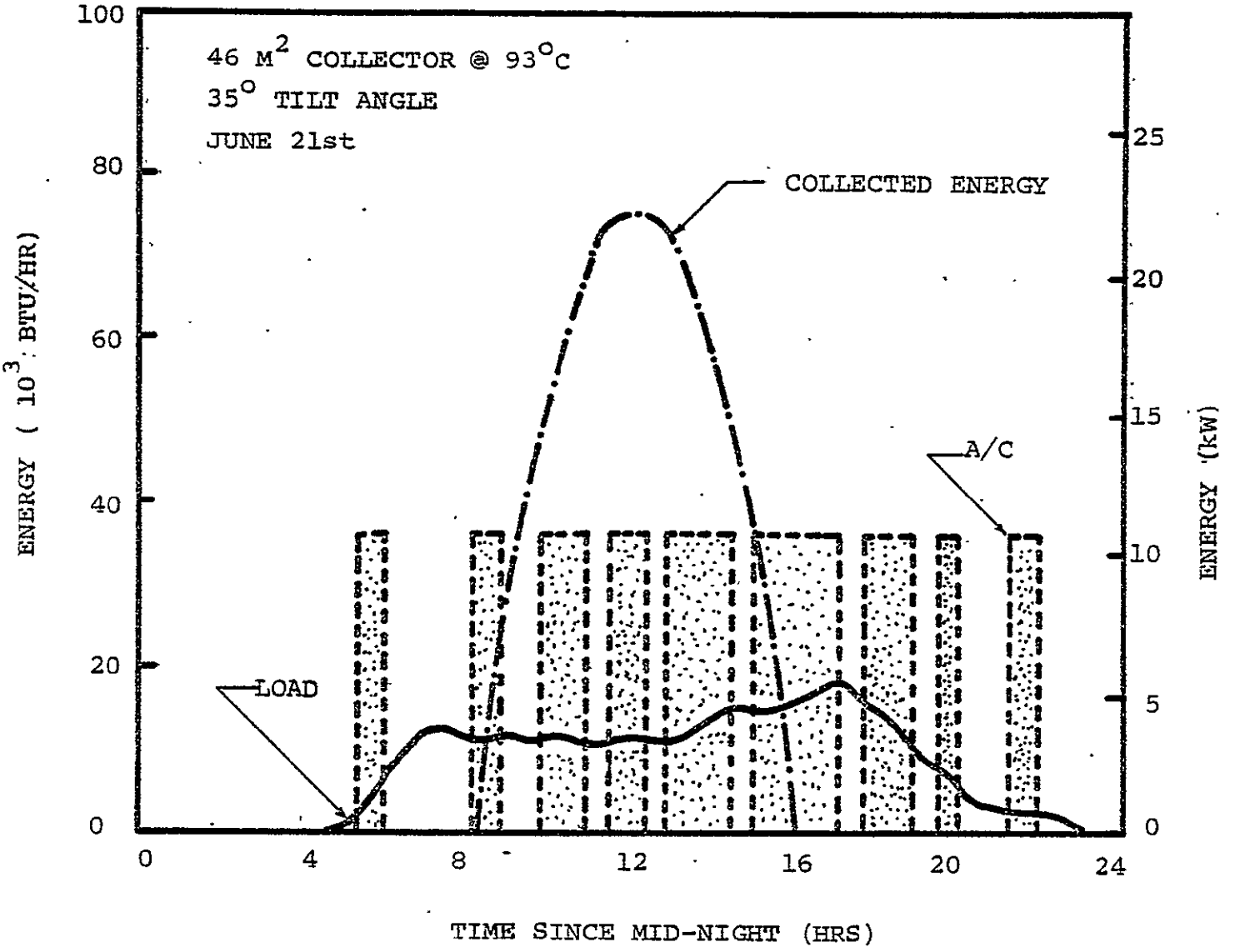

FIGURE 3-2. THERMAL LOAD OF HOUSE, COLLECTOR OUTPUT, AND COOLING SUPPLIED BY ABSORPTION AIR-CONDITIONER DURING A TYPICAL SUNNY DAY IN THE SUMMER.

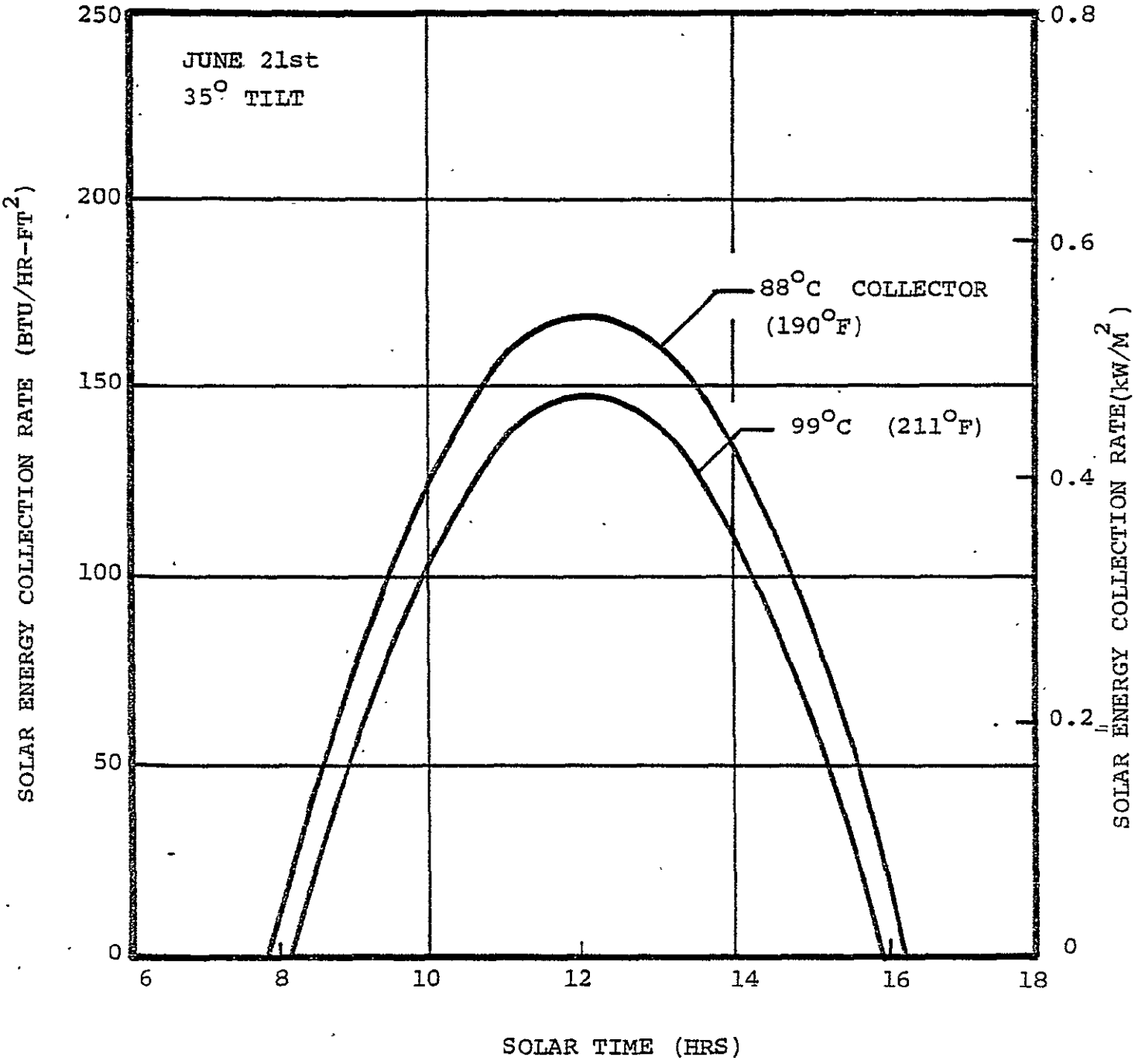

FIGURE 3-3. SOLAR ENERGY COLLECTION RATE FOR COLLECTORS OPERATING IN DAYTIME MODE (99°C) AND NIGHTIME MODE (88°C).

Similar calculations were performed for each of the months in which space cooling is required. These calculations are summarized in Fig. 3-4 where the collector area required to produce 100% of the cooling on a clear day is plotted versus the time of year. The upper curve represents the nighttime cooling mode, while the lower curve represents the daytime mode. For each month the nighttime mode requires 20% to 25% less collector area than the daytime mode.

One familiar aspect of solar cooling systems that is readily apparent in Fig. 3-4 is that relatively small collector areas are needed during most of the cooling season even though large areas are needed druing the peak of the summer. Thus, it is rarely economically justifiable to design a solar cooling system to provide 100% of the energy required. Instead, the optimum design relies on auxiliary energy to supplement the energy provided by smaller collectors during the peak of the cooling season.

This aspect is brought out more clearly in Fig. 3-5 where the percentage of total cooling energy over the entire cooling season is plotted as a function of collector area for the two operating modes. For the diurnal mode a collector area of 710 Ft^2 (66-M^2) is required to provide 100% of the cooling energy over the entire season while a collector with only half this area provides approximately 71% of the cooling energy. Once again one finds that regardless of the percentage of solar cooling, the nocturnal mode presents a distinct advantage over the diurnal mode insofar as required collector area is concerned. For most levels of solar cooling percentage the nocturnal mode requires 20% to 25% less collector area.

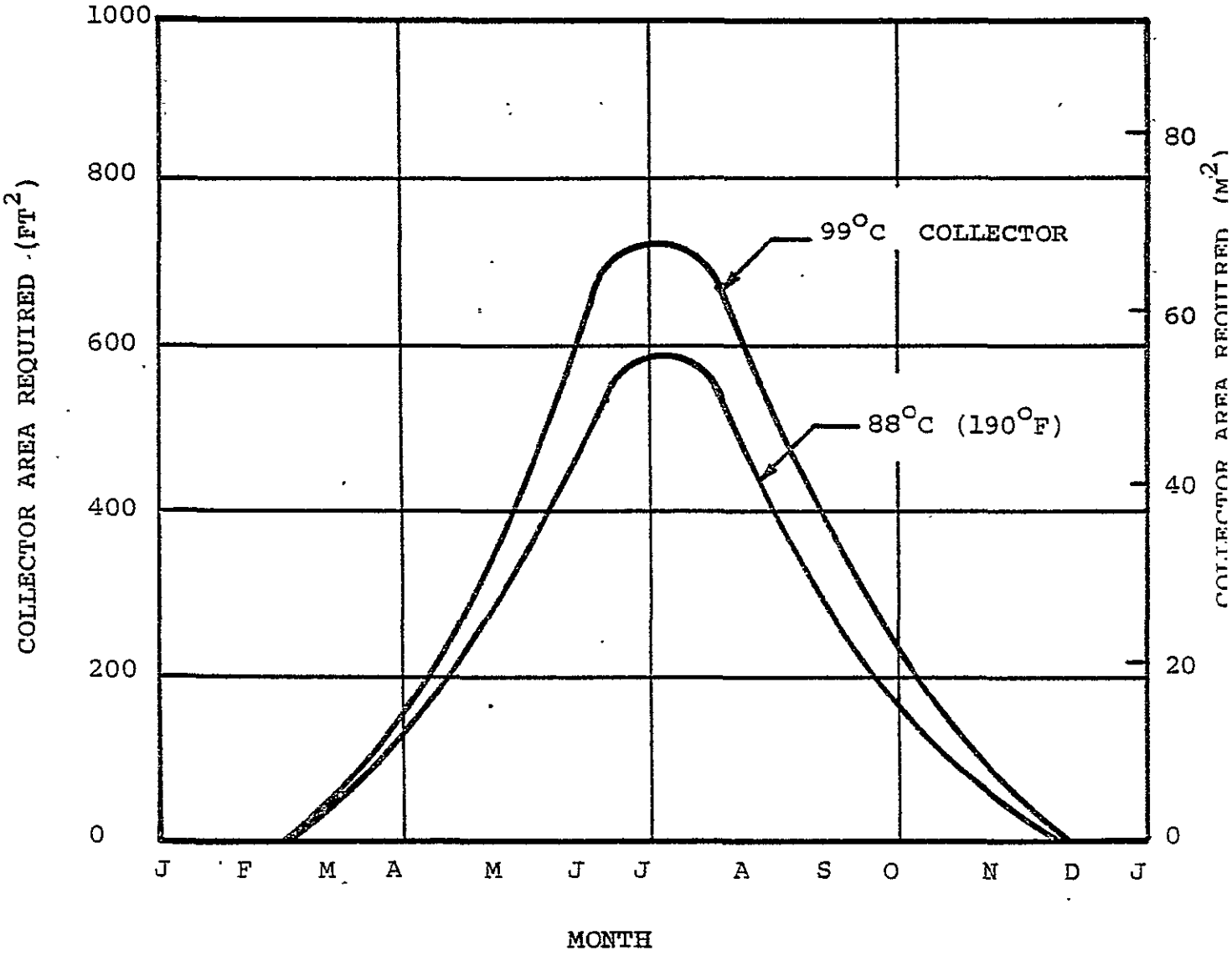

FIGURE 3-4. COLLECTOR AREA REQUIRED TO PROVIDE 100% SOLAR COOLING DURING EACH MONTH.

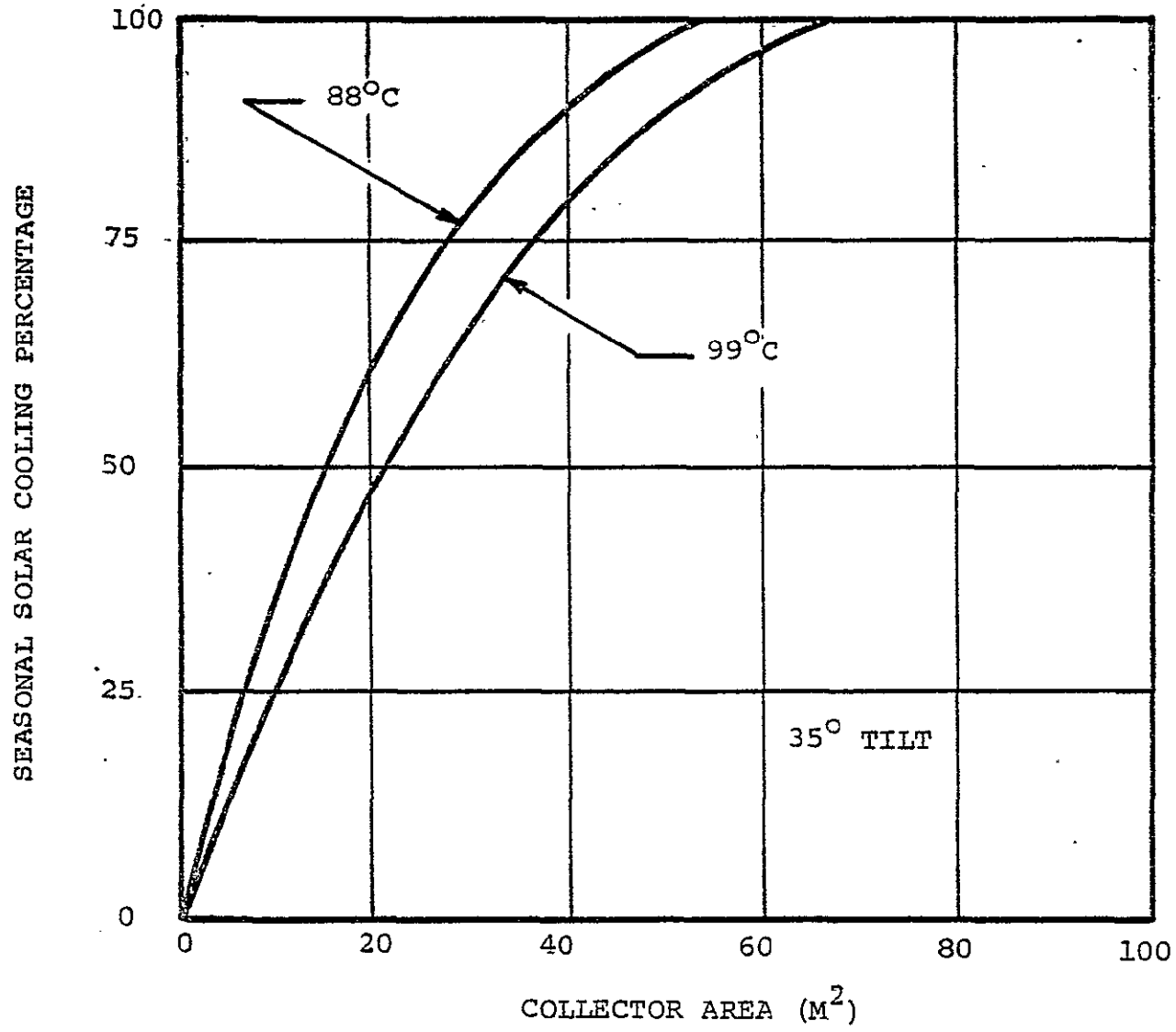

FIGURE 3-5. PERCENTAGE OF SEASONAL COOLING REQUIREMENT PROVIDED BY VARIOUS SOLAR COLLECTOR AREAS FOR DAYTIME (99°C) AND NIGHTTIME (88°C) MODES

In summary, there is little doubt but that the nocturnal cooling mode offers a distinct advantage over the diurnal mode in that smaller collector areas are always required. However, only an economic analysis involving the costs of collectors and storage tanks can determine whether or not the nocturnal mode is truly a more favorable operating mode when all factors are considered.

IV. BOILING HEAT TRANSFER STUDIES

During the study considerable attention was given to improving the design of the generator portion of the lithium bromide absorption cooler. Conventional generator designs incorporate long coils of tubing through which the water heated by the solar collector passes. Since collector efficiency falls off at high opearting temperatures, an optimal absorption cooling system will include a generator which transfers the heat from the collector loop to the absorption cycle loop with as small a temperature difference as is practical. Obviously such an optimization requires detailed knowledge of the heat transfer coefficients associated with various generator configurations. Since little information on this subject is available in the open literature, studies were undertaken to determine heat transfer coefficients for aqueous lithium bromide solutions boiling under two conditions: (1) pool boiling, and (2) falling-film boiling.

A. POOL BOILING STUDIES

Measurements were made of the heat transfer coefficients for heated stainless-steel tubes submerged in aqueous solutions of lithium bromide. The apparatus used for the studies is shown in Fig. 4-1 and Fig. 4-2. It consisted of 0.25 inch (0.64 cm) diameter stainless steel tube containing a uniformly wound resistance heating element. Copper-constantan thermocouples were soldered at locations of one-third and two-thirds of the tube length. A third

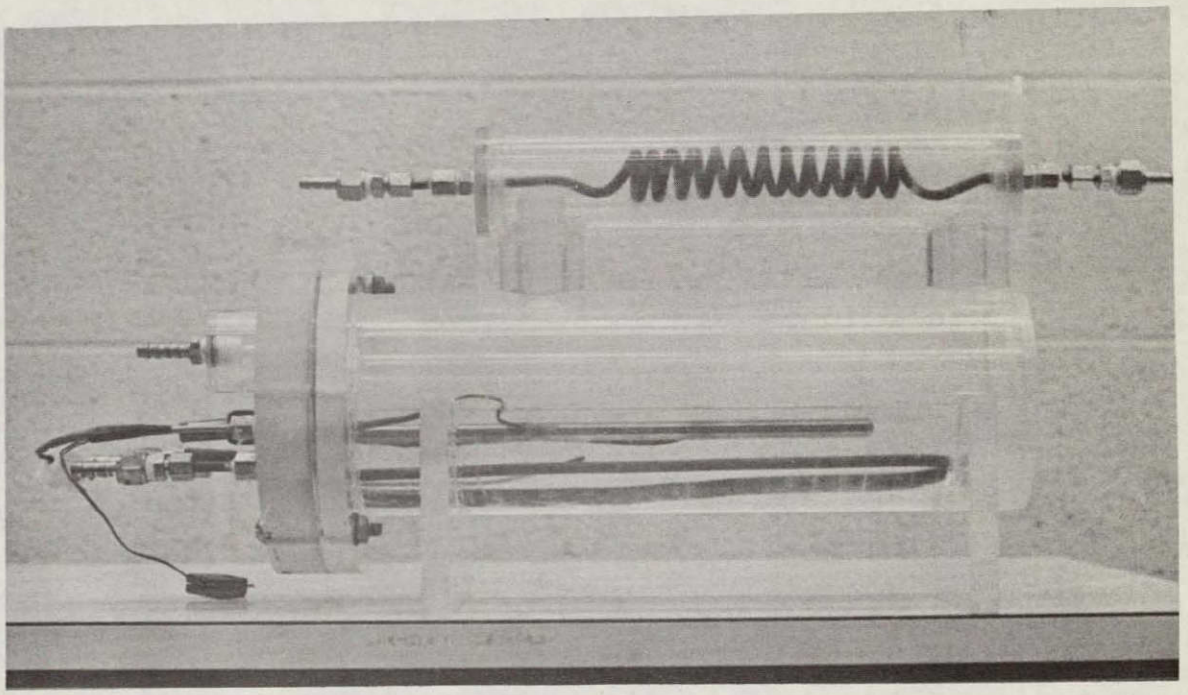

FIGURE 4-1. PHOTOGRAPH OF THE APPARATUS USED IN THE POOL-BOILING STUDIES.

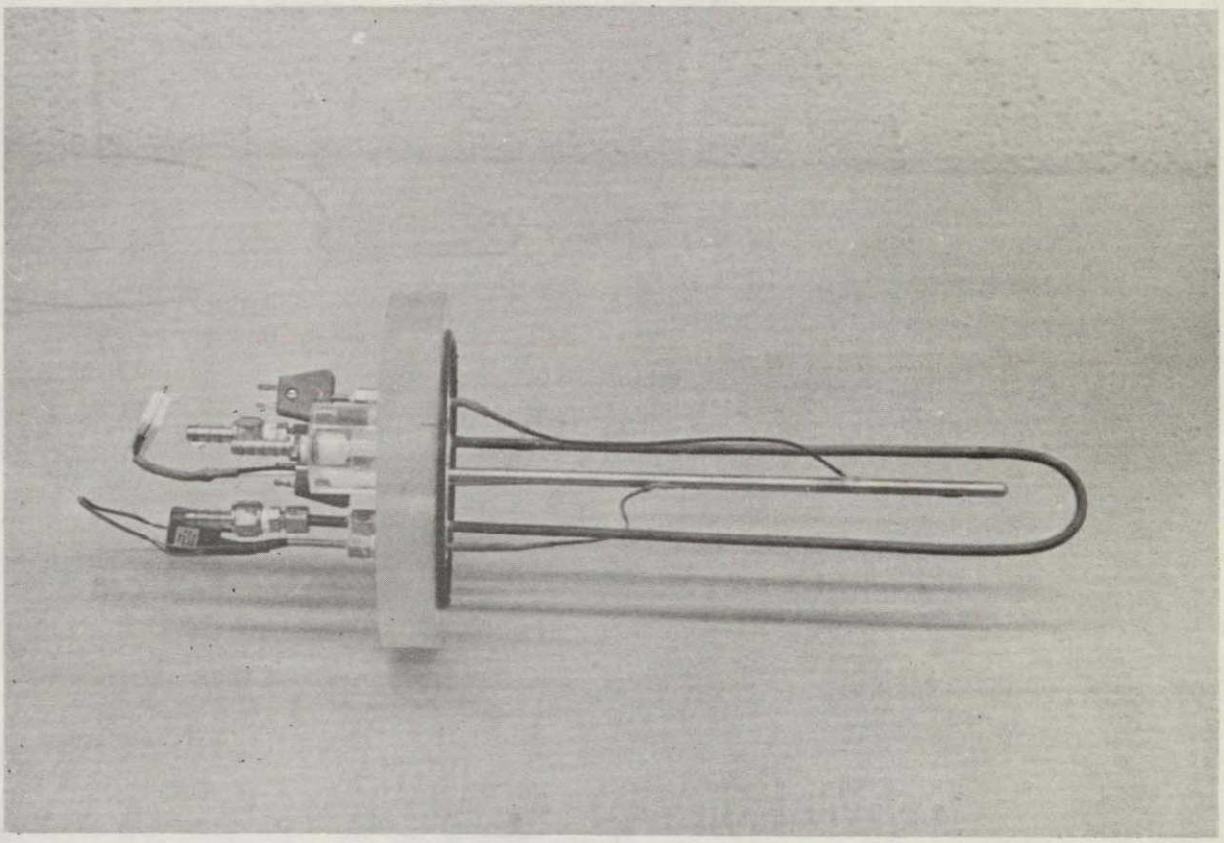

FIGURE 4-2. PHOTOGRAPH OF THE INTERNAL PORTION OF THE BOILING HEAT TRANSFER APPARATUS.

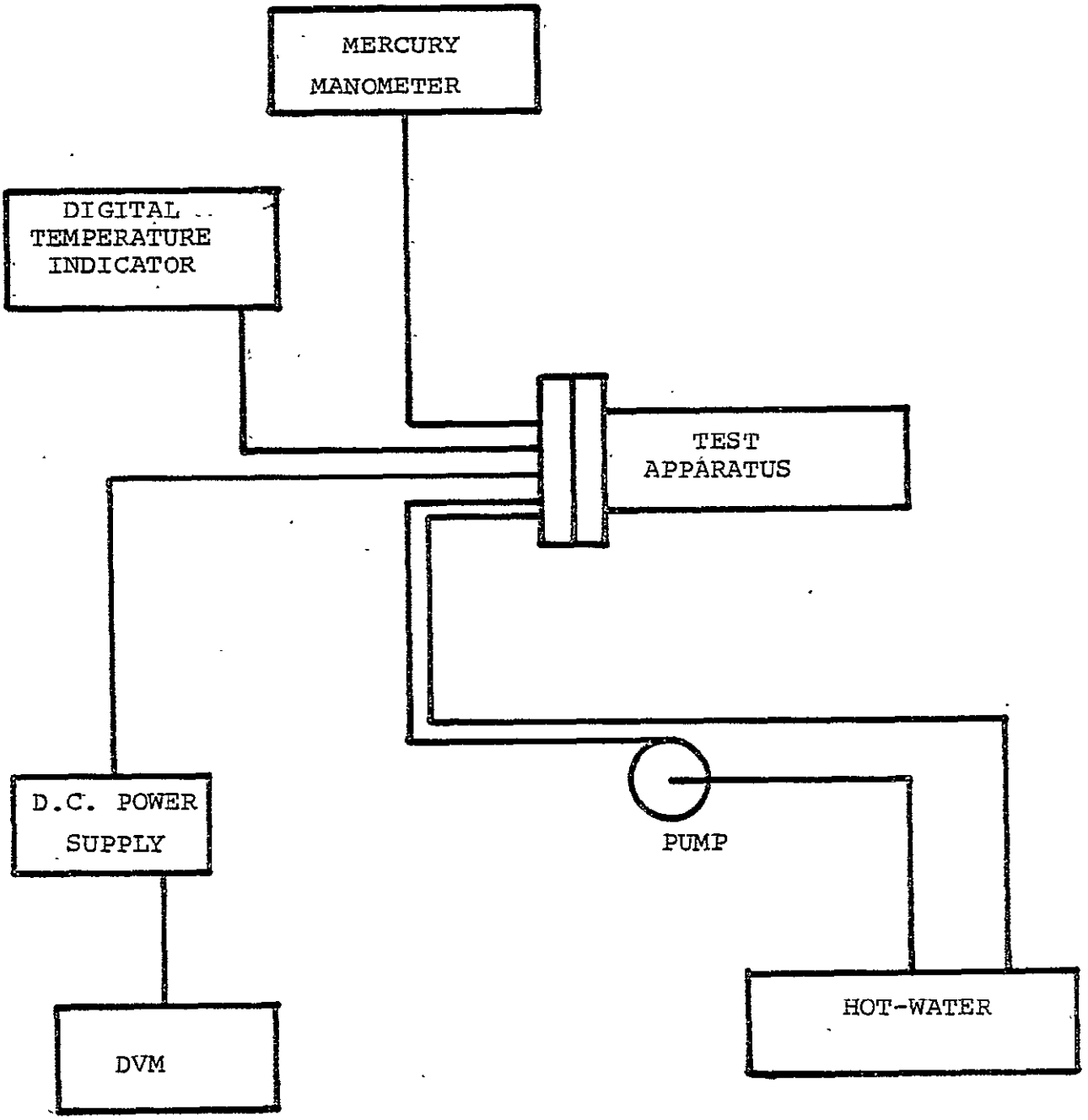

FIGURE 4-3. SCHEMATIC OF TEST SET-UP USED FOR POOL BOILING EXPERIMENTS.

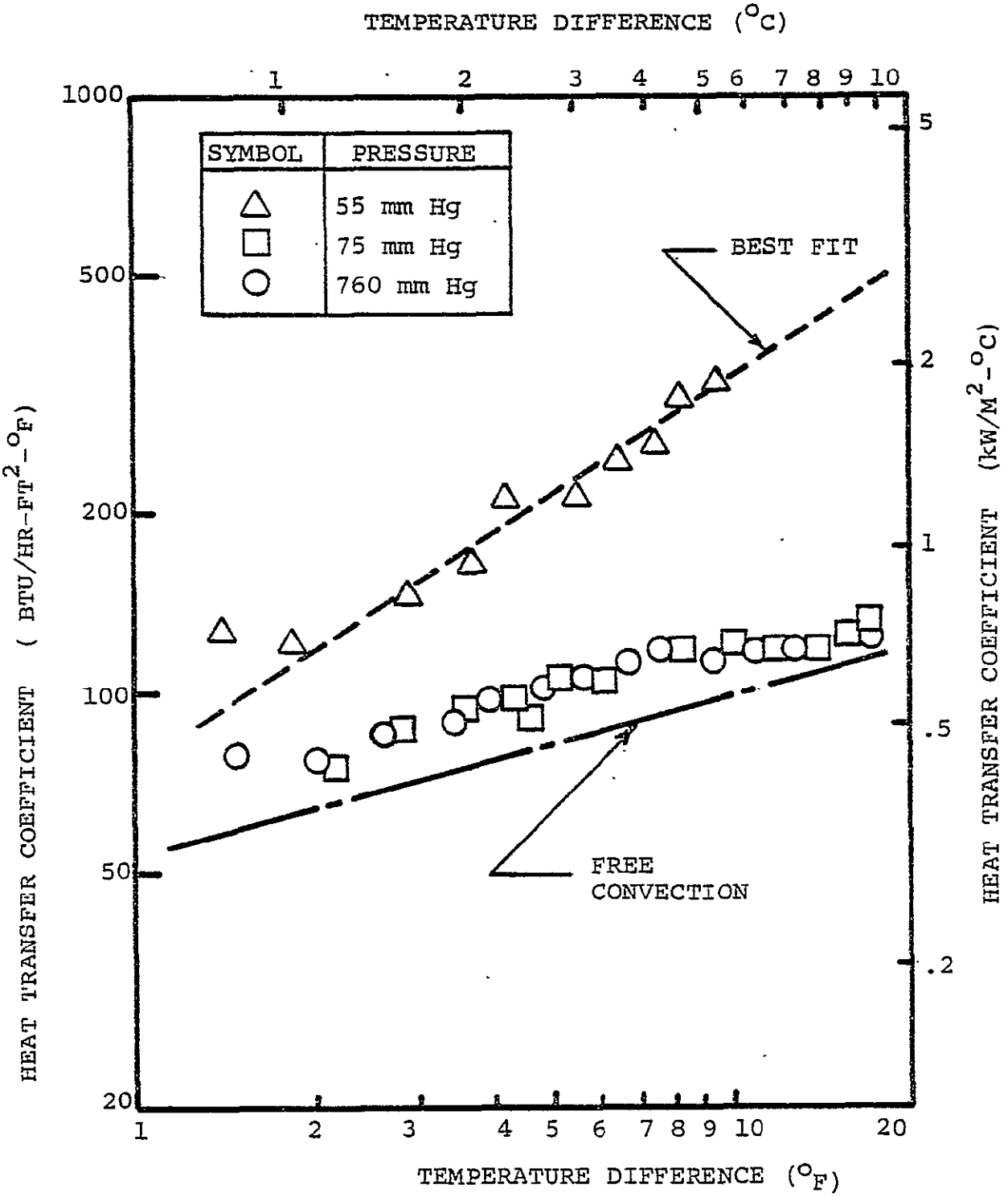

FIGURE 4-4. SUMMARY OF DATA OBTAINED FROM POOL BOILING EXPERIMENTS.

Hg, 75 mm Hg, and 55 mm Hg. In all three cases the solution temperature was maintained at 160°F (71°C).

From Fig. 4-4 it is apparent that the pressure has little effect as it falls from 760 mm Hg to 75 mm Hg. For system pressures in this range the measured heat transfer coefficients correspond very closely to those predicted by free-convection theory {13}, as indicated by the broken line in the figure. Observations of the process for these pressures reveal that relatively little boiling activity occurs for the temperature differentials employed, which ranged from approximately 2°F (1°C) to 18°F (10°C).

Although it is not obvious from the data presented in Fig. 4-4, this same behavior was observed until the pressure was reduced to approximately 55 mm Hg. At that pressure, vigorous bubbling was observed throughout the liquid, indicating a thermodynamically saturated solution. At 55 mm Hg boiling at the heated surface was observed for temperature differences as small as 2°F (1°C) and vigouous boiling was present with temperature differences of 10°F (6°C). As can be seen in Fig. 4-4, this increased boiling activity was accompanied by heat transfer coefficients that were two to three times greater than those observed at elevated system pressures. Additional data revealed that the system pressure must be maintained no higher than 10 mm Hg above saturation if the benefits of vigorous boiling are to be obtained for the temperature differences employed. However, if such near-saturation pressures are maintained, bare submerged-tube generators can operate with

tube-to-solution temperature differentials of only 5 to 10 degrees Fahrenheit (3 to 5 degrees Celsius) and employ outside heat transfer coefficients of approximately 250 Btu/hr-ft^2-^{o}F (1500 W/M-^{o}C). Operating well above saturation pressure at the same temperature differential will result in heat transfer coefficients on the order of 100 Btu/hr-ft^2-^{o}F (600 W/M^2-^{o}C).

Although in a strict sense these results apply only to 50% by weight solutions at 160^{o}F (71^{o}C) heated with 0.25 inch (0.64 cm) diameter stainless steel tubes, there is no reason to expect other operating points to have drastically different characteristics. Thus from the standpoint of absorption system optimization, every effort should be made to eliminate non-equilibrium effects which would prevent near-saturation pressures from being maintained in the generator.

B. FALLING-FILM BOILING HEAT TRANSFER

It has long been known that moderately high rates of heat transfer are often associated with a thin film of liquid falling under gravity over a heated surface. In the past a number of studies {14, 15, 16} have examined falling-film heat transfer for several geometrics and liquids. Since no prior work related to lithium bromide solutions has been reported in the open literature, an analysis of the problem was performed along with a set of experimental investigations.

An analysis of falling film heat transfer as it pertains to

a liquid evaporating as it flows along an inclined heated flat plate was undertaken. The flow geometry considered is shown in Fig. 4-5. Since the problem is essentially the reverse of that of a vapor condensing on an inclined plate, the analysis is very similar to that performed for the problem of filmwise condensation {17}. The following assumptions form the basis for the evapration analysis:

(1) Steady Laminar Flow

(2) Conduction Heat Transfer through the Film

(3) Constant Heated Plate Temperature

(4) Saturated Liquid Film

(5) Negligible Liquid-Vapor Interfacial Shear

(6) Negligible Convective Terms in the Momentum Equation

(7) Newtonian Fluid

Applying Newton's Second Law to an element of liquid and neglecting all forces on the element except the viscous shear force and the weight of the element, the following equation results:

$$\rho g \cos\theta + \frac{\partial \tau}{\partial y} = 0 \qquad (4.1)$$

For laminar flow of a Newtonion fluid,

$$\tau = \mu \frac{\partial v}{\partial y} \qquad (4.2)$$

Thus, within the constraints of the initial assumptions the

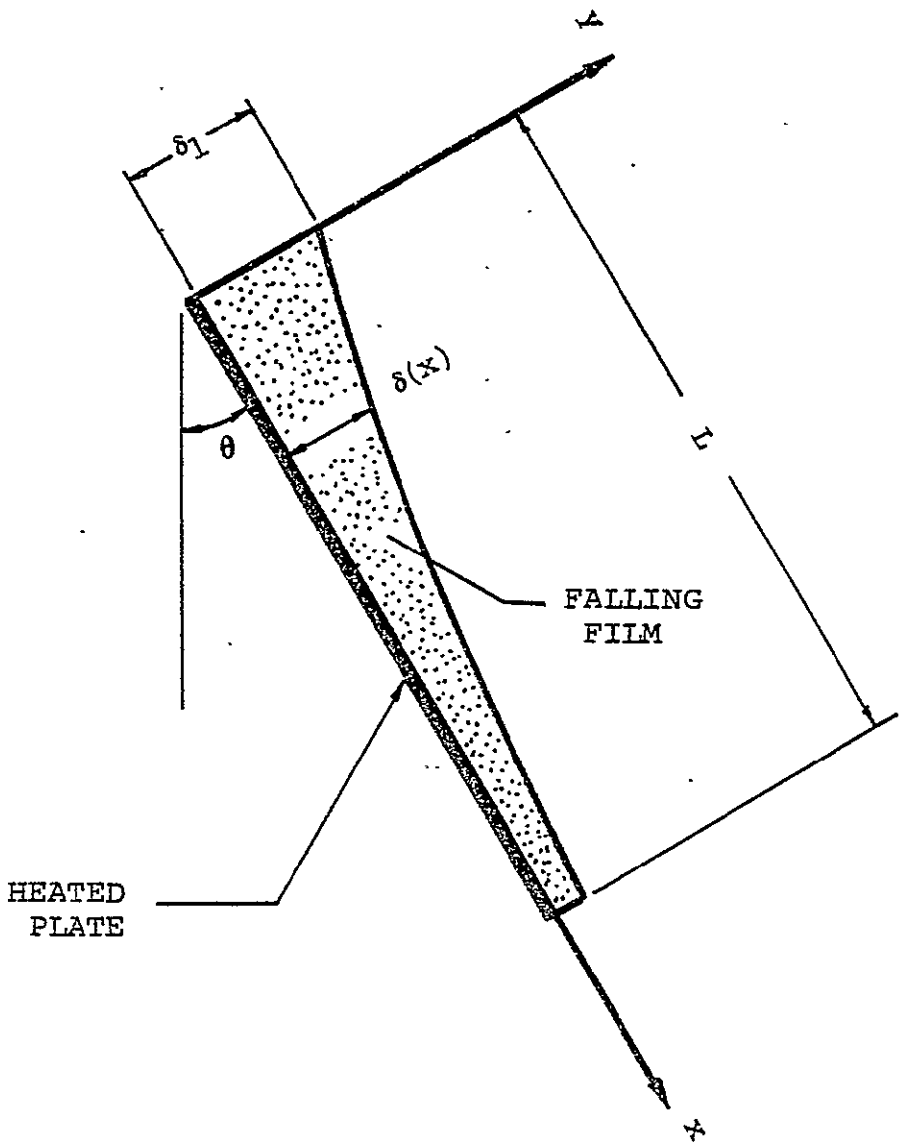

FIGURE 4-5. FALLING-FILM GEOMETRY.

velocity distribution within the liquid is given by

$$\frac{\partial^2 v}{\partial y^2} = -\frac{\rho g}{\mu} \cos\theta \qquad (4.3)$$

subject to the boundry conditions

$$v(x,0) = 0 \qquad (4.4a)$$

$$\frac{\partial v(x,\delta)}{\partial y} = 0 \qquad (4.4b)$$

The first boundary condition is a result of a no-slip condition at the plate while the second condition arises from the assumption of no shear at the liquid-vapor interface (i.e. at $y=\delta$). Integrating Eq. 4.3 and applying the boundary conditions one finds the velocity distribution within the liquid film is given by

$$v(x,y) = \frac{\rho g \delta^2}{\mu} \cos\theta \left\{ \frac{y}{\delta} - \tfrac{1}{2}\left(\frac{y}{\delta}\right)^2 \right\} \qquad (4.5)$$

where $\delta(x)$ is the film thickness at a location x along the plate.

The mass flow rate down the plate is $\Gamma(x)$ where

$$\Gamma(x) = \int_0^{\delta} \rho v(x,y)\, dy \qquad (4.6)$$

Combining Eqs. 4.5 and 4.6, one finds

$$\Gamma(x) = \frac{\rho^2 g \cos\theta}{3\mu} \delta^3 \tag{4.7}$$

As the liquid travels along the plate a distance dx along the plate, vapor evolves at the rate $d\Gamma$ where $d\Gamma$ is simply the change in Γ as the fluid moves to position x to position x + dx. From the above equation

$$d\Gamma = \frac{\rho^2 g \cos\theta}{\mu} \delta^2 \, d\delta \tag{4.8}$$

where $d\delta$ is the corresponding change in the film thickness. Of course, since the vapor is the result of evaporation, the energy required to change Γ by an amount of $d\Gamma$ is

$$dq = -d\Gamma \, h_{fg} \tag{4.9}$$

where h_{fg} is the heat of vaporization for the liquid. The film is assumed to be at the plate temperature at the inner boundary (y=0) and at saturation temperature at the outer boundary (y=δ). Furthermore, it is assumed that heat is transferred through the film purely by conduction. Thus,

$$dq = \frac{k\ (T_{sat} - T_w)}{\delta}\ dx \qquad (4.10)$$

Combining Eqs. 4.8 - 4.10 and applying the condition that at x=0 the film thickness is some initial value δ_1, the following expression for the film thickness along the plate results:

$$\delta(x) = \delta_1 \{1 - \frac{4\mu k(T_w - T_{sat})}{\rho^2 g \cos\theta\ h_{fg}\ \delta_1^4}\}^{\frac{1}{4}} \qquad (4.11)$$

Defining a local heat transfer coefficient h_x as

$$h_x = \frac{dq}{dx(T_{sat} - T_w)} \qquad (4.12)$$

and using Eqs. 4.10 and 4.11, one finds

$$h_x = \frac{k}{\delta}$$

$$= \frac{k}{\delta_1} \{1 - \frac{4\mu k\ (T_w - T_{sat})}{\rho^2 g \cos\theta\ h_{fg}\ \delta_1^4}\}^{\frac{1}{4}} \qquad (4.13)$$

Finally, defining the mean heat transfer coefficient along the plate as

$$\bar{h} = \frac{1}{L}\int_0^L h_x\ dx \qquad (4.14)$$

and carrying out the required integration, the following expression for the mean heat transfer coefficient results:

$$\bar{h} = \frac{\rho^2 g \cos\theta \, h_{fg} \, \delta_1^3}{3\mu(T_w - T_{sat})L} \left\{ 1 - \left\{ 1 - \frac{4\, k(T_w - T_{sat})L}{\rho^2 g \cos\theta \, h_{fg} \delta_1^4} \right\}^{3/4} \right\} \quad (4.15)$$

For most cases of practical interest, this rather cumbersome relation can be greatly simplified since the term subtracted from one in the inner bracket is generally very small compared to unity. Recalling that if ε is very small, then

$$(1 - \varepsilon)^{3/4} \simeq 1 - 3/4\, \varepsilon \quad (4.16)$$

Making use of this result in Eq. 4.15 and collecting terms one finds

$$h \simeq \frac{k}{\delta_1} \quad (4.17)$$

This result should not be surprising since it simply restates the initial assumption that the heat is transferred across the film, whose thickness is approximately δ_1 all along the plate, by conduction. However, from Eq. 4.17 it is apparent that very thin films are necessary if high heat

transfer coefficients are to be obtained. For a 50% solution of lithium bromide at 160°F, for example, heat transfer coefficients on the order of 500 Btu/hr-ft^2-°F (2800 w/m^2-°C) can be obtained if film thickness of approximately 0.007 inch (.17 MM) are maintained.

The film thickness, of course, is determined completely by the mass flow rate down the plate. From Eq. 4.7 it is seen that

$$\delta_1 = \left\{\frac{3\mu}{\rho^2 g \cos\theta}\right\}^{1/3} \Gamma_1^{1/3} \qquad (4.18)$$

where Γ_1 is the initial mass flow rate per unit plate width. Returning to the case cited above, a mean heat transfer coefficient of 500 Btu/hr-ft^2-°F (2800 w/m^2-°C) requires a normalized mass flow rate of 59 lbm/hr-ft (88 kg/hr-m).

As a closing point of interest relative to the falling film analysis, the mean heat transfer coefficient can be expressed as

$$\bar{h} = \left\{\frac{\rho^2 k^3 g \cos\theta}{\mu}\right\}^{1/3} \Gamma_1^{-1/3} \qquad (4.19)$$

by combining the two previous equations. This relation

bears a very strong resemblance to one recommended by McAdams [17] for predicting the mean heat transfer for filmwise condensation on a vertical plate. As discussed earlier, this should not be surprising since the analysis for the falling film is almost identical to that applied to film condensation.

In order to determine the degree of validity of the above analysis, a laboratory apparatus was constructed to conduct falling-film heat transfer investigations. The apparatus was designed so that it could also serve as the generator-condenser portion of a laboratory-scale absorption cooler. A photograph of the device is presented in Fig. 4-6.

The falling film plates were constructed of 0.05-inch (.13 cm) thick brass sheet and measured 5 inches (12.5 cm) in width and 11 inches (28 cm) in length. An inclination angle of approximately 10^{o} was provided to prevent detachment of the film as it traveled down the plate. A quarter-inch (0.64 cm) diameter copper tube was soldered on the back of each plate in serpentine fashion and carried hot water which supplied the necessary heat to the plate. Lithium bromide solution was pre-heated by the hot water and then introduced at the top of each plate via five small holes drilled into a stainless steel flow-distributing tube. The liquid leaving the plate passed through the drain at the bottom of the stainless steel housing and was recirculated by means of a small pump. The water vapor produced by the

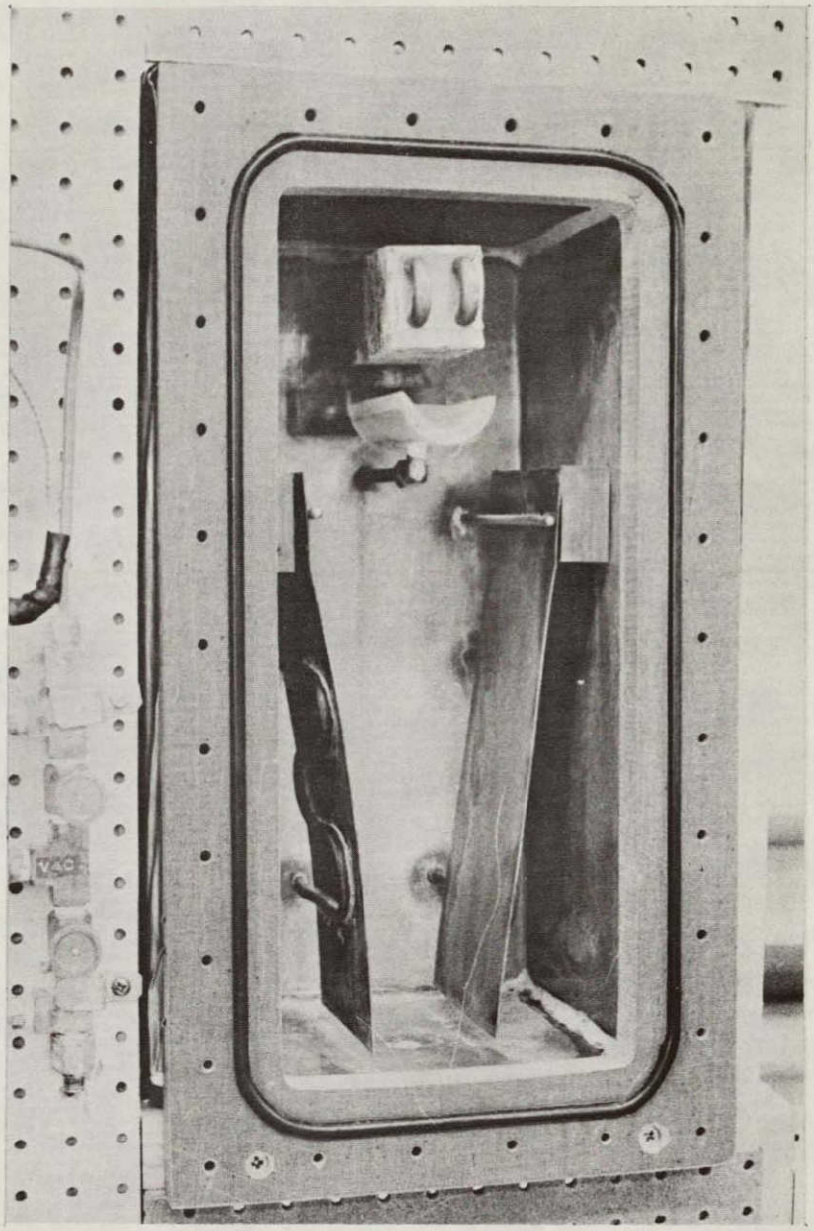

FIGURE 4-6. PHOTOGRAPH OF THE FALLING-FILM HEAT TRANSFER APPARATUS.

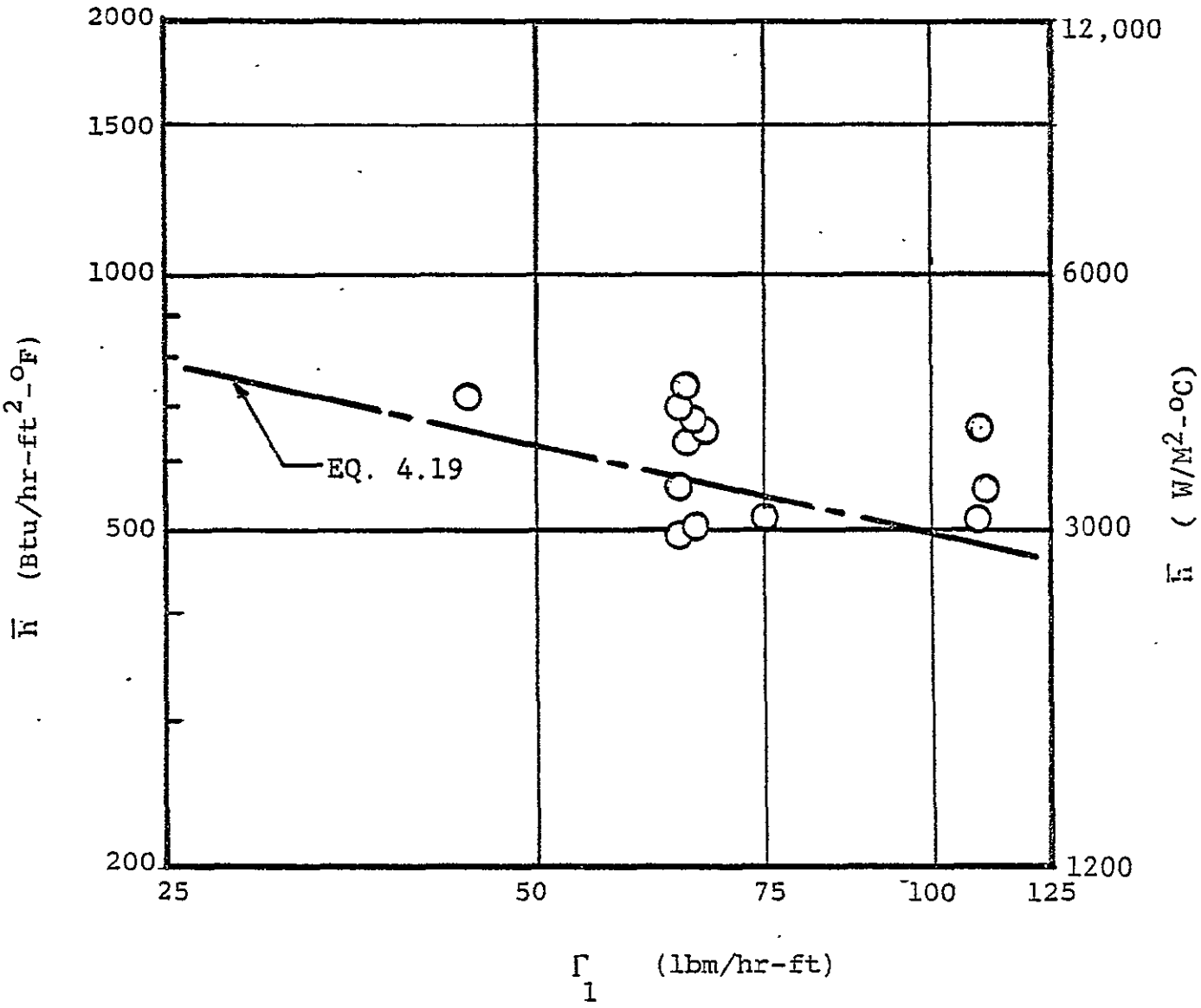

FIGURE 4-7. EXPERIMENTAL AND THEORETICAL VALUES OF FALLING-FILM HEAT TRANSFER COEFFICIENTS AS FUNCTIONS OF INITIAL FLOW RATE.

other geometries besides flat plates. A particularly intriguing geometry is one in which the fluid film falls down the outer surface of a cone. If the conical surface were properly prepared, the film would wet the entire surface which would cause the film thickness to become quite small as the fluid approached the bottom of the cone. Assuming laminar flow exists, the process would once again be governed by conduction through the film. A relation similar to Eq. 4.17, except that the initial film thickness would be replaced by some average thickness, could be expected to describe the heat transfer process. Consequently, heat transfer coefficients several times larger than those found in the present investigations could be obtained.

In summary, falling-film heat transfer offers an attractive approach to generator design in solar absorption equipment and should be given further consideration in the future.

V. LABORATORY-SCALE ABSORPTION COOLER

From the outset of the study it was intended to construct a laboratory-scale absorption unit to determine the effects of various component changes and operating temperatures on the overall system performance. Because of a number of problems, which centers primarily around obtaining an effective absorber, this portion of the program was only partially successful. Fortunately, the limited success experienced in this phase of the study did not hamper the progress of the other phases.

The philosophy underlying the design of the laboratory-scale cooler was to provide a well instrumented unit capable of frequent modification and which permitted direct observation of the internal operation of the components. Consequently, the decision was made to fabricate the generator, condenser, evaporator, and absorber as four separate units and to use a transparent acrylic material as the exterior housing material for each.

Table 5-1 summarizes the principal design parameters for the initial system. Figure 5-1 shows the basic lay-out of the system and the instrumentation provided, and Fig. 5-2 presents a photograph of the system before all of the inter-connecting piping was installed.

The generator consisted of three 45 inch (114 cm)

GENERATOR	
Heat Input	3400 BTU/HR (1.0 kw)
Water Inlet Temperature	150°F (66°C)
Water Outlet Temperature	147.5°F (64°C)
Solution Inlet Temperature	131°F (55°C)
Solution Outlet Temperature	140°F (60°C)
Solution Inlet Concentration	49% LiBr
Solution Exit Concentration	52% LiBr
Solution Flow Rate	52 LBM/HR (114 KG/HR)
EVAPORATOR	
Cooling Output	3000 BTU/HR (.88 kw)
Chill Water Inlet Temperature	80°F (27°C)
Chill Water Outlet Temperature	77°F (25°C)
Refrigerant Temperature	55°F (13°C)
Refrigerant Flow Rate	2.9 LBM/HR (6.4 KG/HR)

TABLE 5-1. DESIGN PARAMETERS FOR EXPERIMENTAL ABSORPTION COOLING SYSTEM

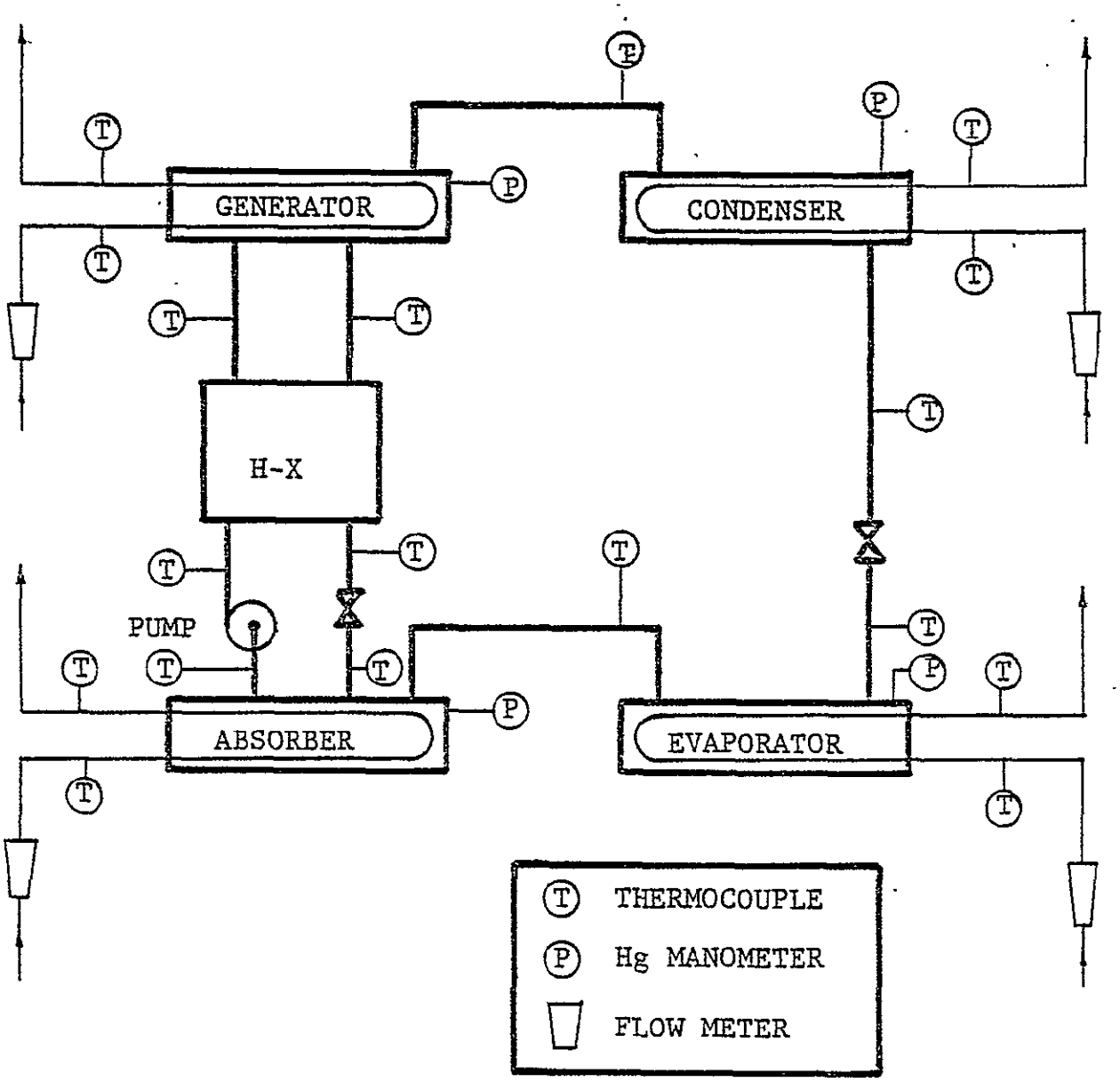

FIGURE 5-1. LAY-OUT OF LABORATORY-SCALE ABSORPTION SYSTEM AND THE INSTRUMENTATION SYSTEM EMPLOYED.

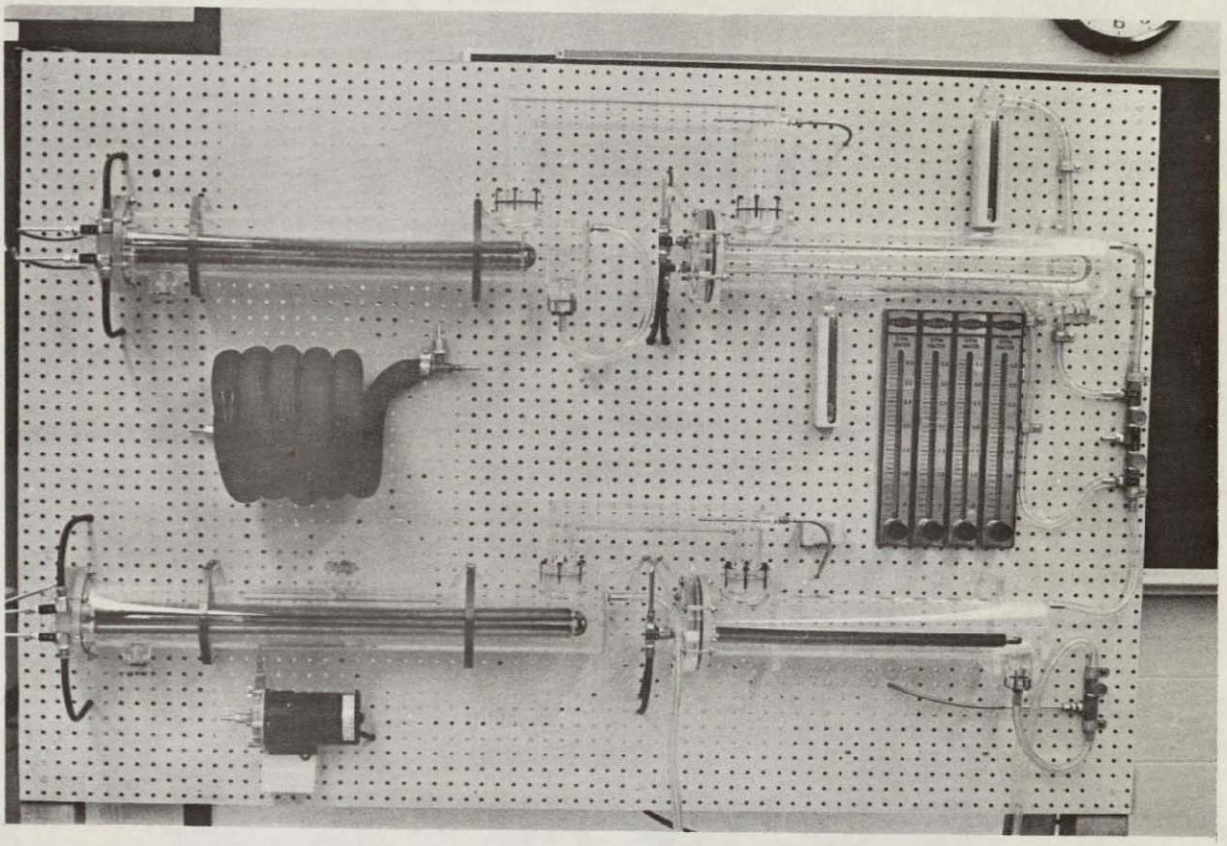

FIGURE 5-2. PHOTOGRAPH OF THE INITIAL LABORATORY-SCALE ABSORPTION COOLER.

diameter acrylic tube was once again used as the housing.

Since the entire system operated under a moderate vacuum (10 to 50 mm Hg), vacuum leaks proved troublesome at first. These were often due to poor connections between the acrylic housing and metal fittings. However, as time passed, these problems grew to be less and less of an annoyance and did not significantly hinder the overall progress.

Despite the fact that the generator, condenser, and evaporator performed much as expected, all attempts to operate this initial system as a complete cycle failed. Close examination revealed that this failure could be attributed almost completely to the inability of the absorber to re-absorb satisfactorily the refrigerant vapor produced in the evaporator. Consequently, efforts began to modify the absorber, and these efforts continued through the remainder of the program.

To provide some sense of direction, a few very elementary experiments were performed to determine the rate of absorption rate of water vapor by lithium bromide solution. Open beakers of water and lithium bromide (54% concentration) were placed in a bell jar and the space was evacuated to a pressure corresponding to the saturation pressure of water at room temperature. Some time later the vacuum was released, and the amount of water absorbed

by the solution was determined by weighing the latter. If the absorption rate is assumed to be proportional to the product of the free surface areas of the two liquids, the experiments indicated a proportionality constant of approximately 0.8 lbm/hr-ft^4 (.002 gm/hr-cm^2). Assuming this value, the initial absorber design at best could have provided a re-absorption rate on the order of 0.3 lbm/hr, which is only about one-tenth of the required value. To achieve even this value there would have had to have been no impediment offered the refrigerant vapor along its path from the evaporator to the absorber. Since the initial path was via a 1.5-inch (3.8 cm) diameter acrylic tube connecting the absorber and evaporator shells, it is very doubtful that even this low rate of vapor re-absorption could have been realized.

To alleviate these deficiencies, a new absorber was designed, fabricated, and installed in the system. Figure 5-3 presents a schematic of the modified system. To reduce any flow impediments between the evaporator and absorber, the two components were housed in a single 6" (15 cm) diameter acrylic shell. The larger shell increased the surface area available for re-absorption by approximately 100 %. However, the major modification introduced to enhance refrigerant re-absorption was an array of three spray bars (one vertical and two horizontal) through which lithium

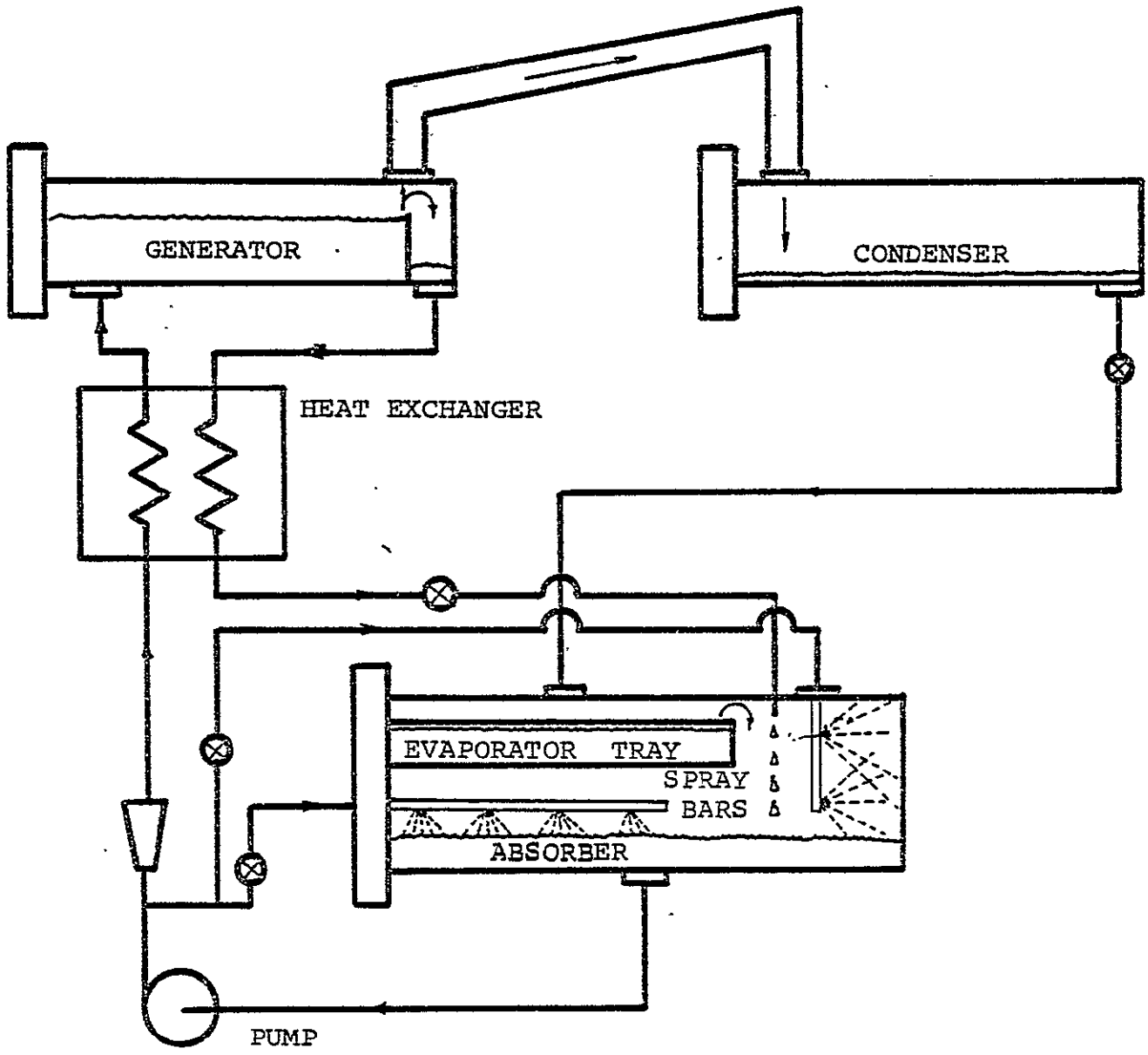

FIGURE 5-3. SYSTEM CONFIGURATION WITH MODIFIED ABSORBER.

bromide solution was recirculated through the absorber.

Although this unit did not perform completely satisfactorily, it did permit a limited amount of encouraging data to be obtained. For example, in one series of tests the evaporator tray was filled with water at 70°F while a 54% solution of lithium bromide was introduced into the absorber section. The absorber/evaporator unit was isolated from the rest of the system and the pressure inside the unit was reduced to approximately 20 mm Hg by means of a vacuum pump. As the lithium bromide solution began to absorb the water vapor present additional vapor evolved from the evaporator tray, causing the temperature of the remaining water to fall. A number of tests were conducted with the system operating in this intermittent mode. Evaporator temperatures as low as 55°F (13°C) were obtained with no recirculation flow through the spray bars, and temperatures as low as 45°F (7°C) were observed with the spray bars in use. Thus, the modifications introduced into this second absorber design were definitely beneficial in promoting the re-absorption rate of the refrigerant vapor by the absorbent. Unfortunately, the re-absorption rate was still too low to permit continuous operation of the entire absorption system. All attempts to operate the system in a continuous fashion resulted in failure.

In a final attempt to obtain steady operation, a third absorber design evolved. The basic principle of the design is shown in Fig. 5-4. The lithium bromide solution is again recirculated through the absorber, but this time the liquid flows down a series of tilted plates in a cascade fashion. Cooling water passing through tubes bonded to the backs of the plates removes the heat produced in the vapor re-absorption process. This absorber is intended to be used with a direct-expansion evaporator coil, although a submerged cube evaporator could be incorporated with the absorber housing. The rationale behind this approach is simply that the large area over which the recirculating fluid is spread combinded with the splashing of the fluid as it falls from one plate to the next should provide good opportunity for re-absorption.

A unit based on this approach was fabricated and is shown in Fig. 5- 5 The plates and shell were fabricated of stainless steel, and an acrylic plate was used for the front cover. Very little use was made of this apparatus, however, because the liquid failed to wet the tilted plates sufficiently to promote a thin uniform film. Instead the fluid tended to trickle down the series of plates. Additional examination of this approach in the future, however, may prove fruitful.

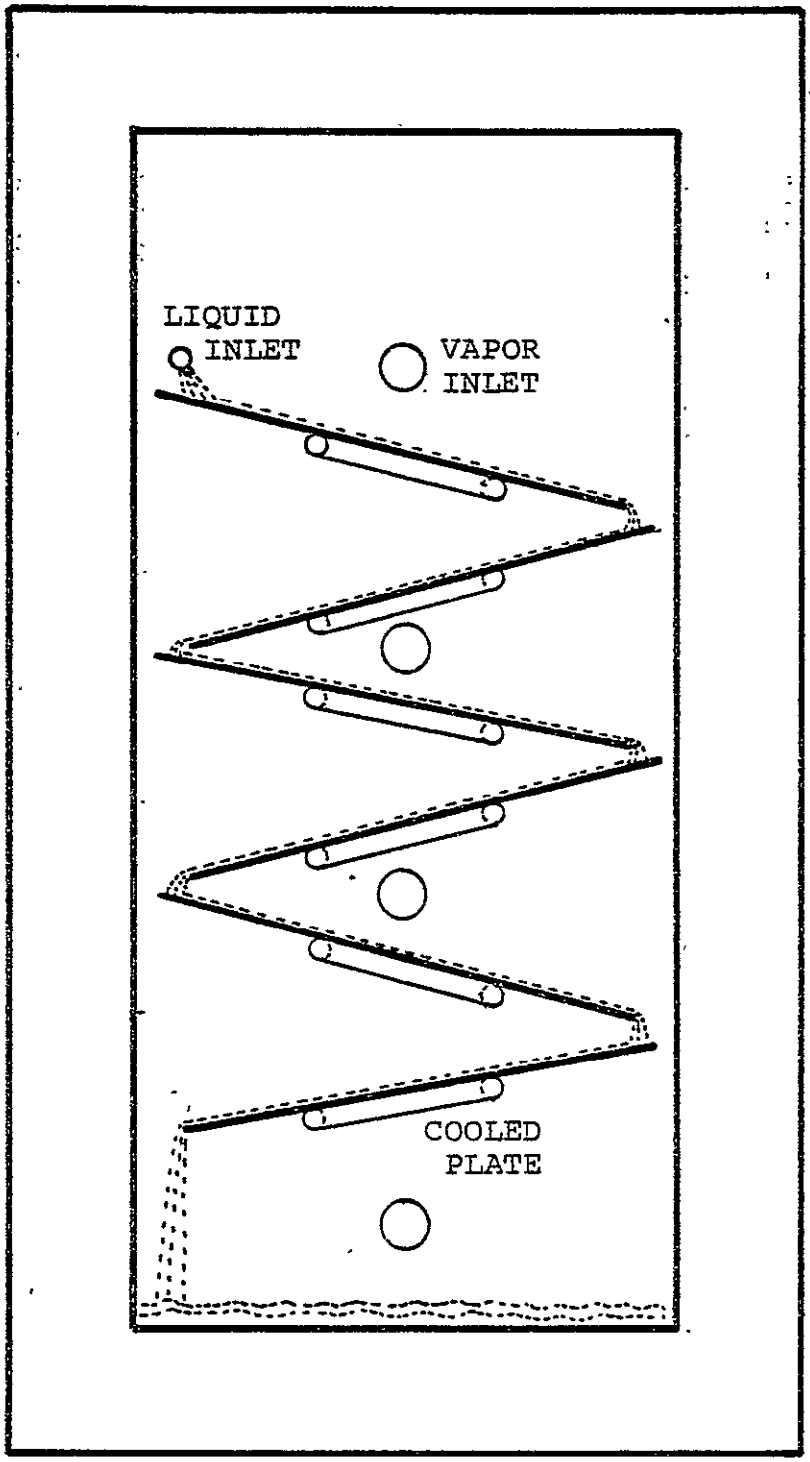

FIGURE 5-4. CASCADE ABSORBER DESIGN.

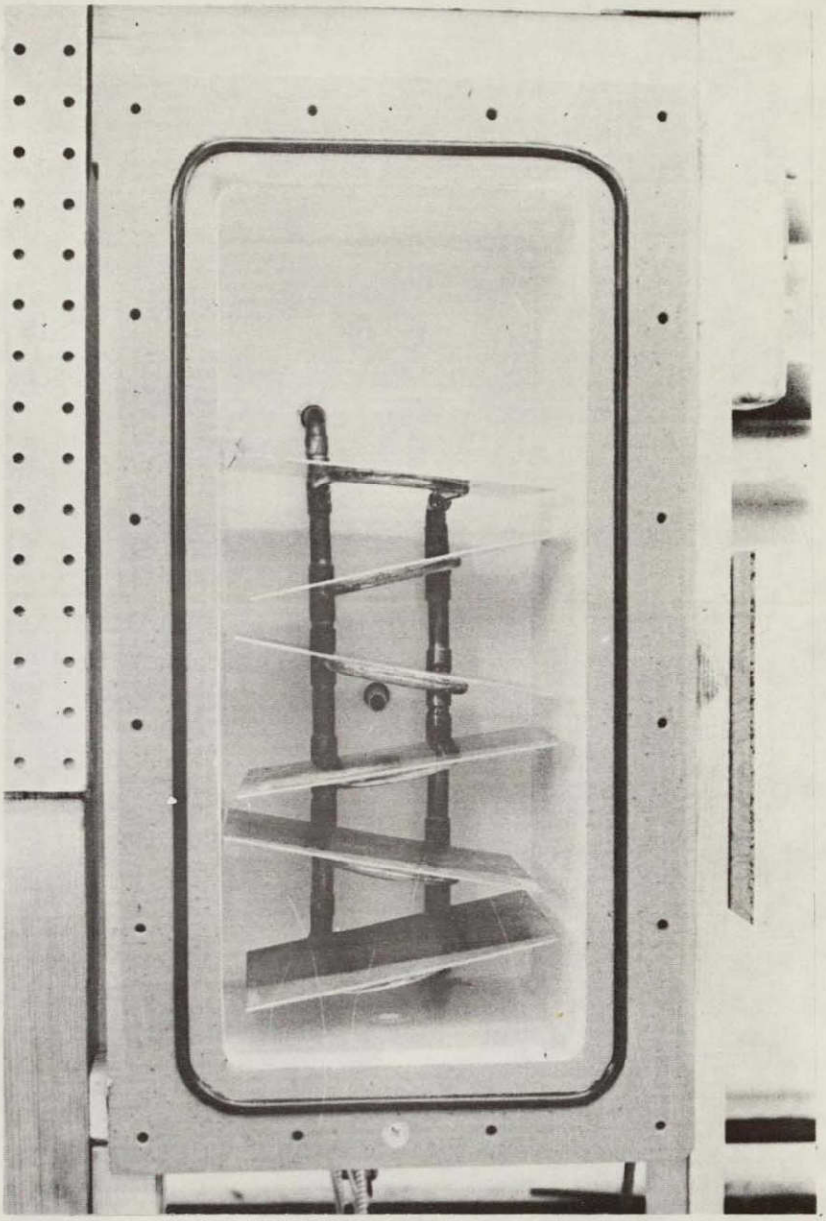

FIGURE 5-5. PHOTOGRAPH OF THE CASCADE ABSORBER.

VI. COLLECTOR CONVECTION SUPPRESSION SURVEY

In a typical flat-plate collector energy is lost from the absorber panel to the environment by convection and radiation. Radiative losses are generally minimized through the use of selective surfaces which absorb radiant energy well in the 0.3 - 3.0 micron range but which emit energy poorly at longer wavelengths. For a collector operating at 100° C with a single cover, a selective surface on the absorber panel can reduce the losses by 50%.

In collectors employing a selective surface, convection represents the major energy-loss mechanism. Two basic approaches have been taken to reduce convective losses in collectors. The first is to evacuate the space between the absorber and the transparent covers. Speyer {18} showed that vacuums lower than 10^{-3} Torr are needed to eliminate convection and conduction. This approach has been incorporated into tubular collectors produced by Owens-Illinois, Inc. and Corning Glass Works {19-20}. In addition, Eaton and Blum {21} found that moderate vacuums (1-25 Torr) combined with selective coatings significantly improve the performance of flat-plate collectors. Such vacuums eliminate convection but still permit conduction through the air space.

A second approach to convection suppression is to introduce honeycomb structures into the space between the absorber and cover. Hollands {22} and Edwards {23} studied

horizontal systems with upward heat flow and found honeycombs to be effective convection suppression devices. Charters and Peterson {24} considered the case of an inclined air layer and found that fluid motion exists for any finite temperature difference between the absorber plate and the cover even when a honeycomb structure is present. They concluded that honeycombs would be of little value in suppressing convection in inclined collectors, although no measurements of the heat transfer were reported.

These and other studies were discussed in some detail by Hollands and Konicek {25}, who experimentally investigated the stability of differentially heated inclined air layers. They brought out the following points. Horizontal air layers heated from below remain stagnant for Rayleigh numbers less than 1708 where the Rayleigh number is defined as the product of the Prandtl number and the Grashof number based on the layer's thickness. The heat transfer across the stagnant layer occurs by conduction. For Rayleigh numbers above 1708 the top-heavy air layer becomes unstable and fluid motion occurs in the form of the well-known hexagonal Benard cells. Once this fluid motion begins, the heat transfer across the layer occurs by natural convection. A honeycomb array can be quite effective in suppressing these convection currents by exerting a restoring shearing force on the fluid as it attempts to begin its cellular motion. For example, it has been shown {22} that a square honeycomb with a height-to-width

ratio of three should suppress convection in a horizontal layer for Rayleigh numbers below 209,000.

With inclined air layers, however, the situation is quite different. For such layers fluid motion exists for very small Rayleigh numbers and is similar to that encountered in a vertical slot and examined by Batchelor{26}. In slot flow at low Rayleigh numbers the fluid motion is laminar, consisting of air rising along the warm wall and falling along the cool wall. Because the flow is laminar, the heat transfer across the layer is essentially by conduction. Thus, in this so-called "base flow" regime, which exists up to Grashof numbers of approximately 10^4, fluid motion occurs but natural convection is still absent. For Grashof numbers above 10^4, this base-flow becomes hydrodynamically unstable and natural convection sets in.

For inclined systems employing honeycombs it is felt that the base-flow within each cell of the honeycomb array remains stable up to some critical Rayleigh number, which depends on the aspect ratio of the honeycomb cell and the angle of inclination. Below this critical Rayleigh number the heat transfer occurs by conduction just as it does in the case of the vertical slot. Above the critical value the flow becomes unstable and convection occurs. The validity of this argument was recently borne out experimentally by Cane et al.{27}. These studies found that square honeycomb arrays with a height-to-width ratio of three suppressed convection up to Rayleigh

numbers of 150,000 for horizontal layers. In addition, for layers inclined at 45^{o} and 60^{o} convection suppression was observed for Rayleigh numbers up to 90,000 and 60,000, respectively. Above these critical Rayleigh numbers the heat transfer across the layer approached that observed when no honeycombs were present. For the cases examined Rayleigh numbers on the order of 10^{6} had to be present before the honeycomb became totally ineffective in reducing the convective heat transfer.

One final study which deserves mention is that by Buchberg and Edwards [28] which examined the use of cylindrical glass honeycombs to improve the performance of flat plate solar collectors. Of particular interest is the fact that this study provides design criteria for incorporating glass honeycombs into flat plate collectors.

Glass honeycombs improve the performance of solar collectors two ways. First, they reduce the convective heat transfer between the absorber and the collector cover. Second, they reduce the infra-red radiation heat transfer from the absorber to the cover. The latter occurs because the glass walls of the honeycomb absorb much of the infra-red radiation emitted by the absorber. When this energy is re-emitted by the glass honeycomb walls, approximately half is directed back toward the abosrber. Naturally, the greater the honeycomb height-to-diameter ratio, the more important is this effect.

Although the honeycomb can improve the collector perfor-

mance, it can also degrade the performance. First, it absorbs and reflects a portion of the incoming solar radiation, thus reducing the energy available to the absorber. This is particularly important for radiation arriving at high angles of incidence. Second, conduction from the absorber to the collector cover occurs through the thin honeycomb walls. For small honeycomb heights this heat loss becomes appreciable.

Buchberg and Edwards concluded that honeycomb diameters less than 0.5 inch (1.27 cm) are required to suppress convection for high operating temperature differentials, and that honeycomb heights greater than 1.0 inch (2.5 cm) are necessary to prevent unacceptably high heat conduction through the glass walls. They also found that height-to-diameter ratios less than approximately 4.0 result in poor infra-red emission suppression, and that ratios greater than 10 reduce the fraction of incident energy that reaches the absorber to an unacceptably low value. Thus, a typical glass honeycomb array for use in flat plate collectors might have a height ranging from two to four inches (5 to 10 cm) and a cell diameter ranging from one-quarter to one-half inch (0.6 to 1.2 cm).

Buchberg and Edwards carried out a theoretical comparison of a conventional single-glazed collector employing a selective absorber and a single-glazed collector employing a glass honeycomb array. The array consisted of 9.3 mm diameter cylinders with a height-to-diameter ratio of 7.3. The honeycomb collector was found to have superior performance character

istics all year with particular improvement during the noontime hours and at high operating temperatures. Furthermore, the studies of Buchberg and Edwards also revealed that honeycomb collectors can be cost competitive with conventional flat plate collectors. The higher initial costs of honeycomb collectors is more than offset by their superior performance characteristi

Thus, it appears that honeycombs do indeed offer one means of improving the performance of flat plate collectors and furth studies of these devices should be carried out in an attempt to optimize the overall collector design.

REFERENCES

1. Terrestrial Application of Solar Technology and Research. NASA Cr-129012, (1973)

2. J. A. Duffie et al, "A Study of a Solar Air Conditioner, Mechanical Engineering, Vol. 85, No. 8, pp 31-39, (1963)

3. P. J. Wilbur and C. E. Mitchell, "Solar absorption air conditioning alternatives," Solar Energy, Vol.17, No. 3, pp 193-200, (1975).

4. R. L. Oonk et al, "Modeling of the CSU heating/cooling system", Solar Energy, Vol. 17, No. 1, pp 21-28, (1975)

5. L. W. Butz et al, "Simulation of a solar heating and cooling system", Solar Energy, Vol. 16, No. 3/4, pp 129-136, (1974).

6. G. O. G. Löf and R. A. Trybout, "The design and cost of optimized systems for residential heating and cooling by solar energy," Solar Energy, Vol. 16, No. 1, pp 9-18, (1974).

7. D. Pogany, D. S. Ward, and G. O. G. Löf, "The economics of solar heating and cooling systems," Paper 21-1, ISES 1975 Solar Energy Conference and Exposition, Los Angeles (1975).

8. G. W. Braun et al, "Assessment of Solar heating and cool for an electric utility company, "Paper 1205, ISES(1975 Solar Energy and Exposition, Los Angeles, (1975).

9. D. S. Ward and G. O. G. Löf, "Design and construction of a residential solar heating and cooling system, "Sola Energy, Vol. 17, No. 1, pp 13-20, (1975).

10. D. Prigmore and R. Barber, "Cooling with the sun's heat. Design considerations and test data for a Rankine cycle prototype," Solar Energy, Vol. 17, No. 3, pp 185-192, (1975).

11. R. T. Ellington et al, The Absorption Cooling Process, Institute of Gas Technology Research Bulletin 14, Chicag (1957.)

12. E. H. Perry, "Theoretical Analysis of Continuous and int mittent lithium bromide-water absorption refrigeration cycles," NASA CR-120336, pp 18-1 - 18-21, (1974).

13. F. Kreith, Principles of Heat Transfer, 3rd Ed., Intext Educational Publishers, (1973).

14. W. H. McAdams et al, "Heat Transfer to falling-water films," Trans. ASME, Vol. 62, pp 627-631, (1940).

15. N. Portalski, Chemical Engr. Science, Vol. 19, pp 575-582, (1964).

16. Thomas and Portalski, Industrial and Engineering Chemistry, Vol. 50, pp 1081-1088, (1958).

17. McAdams, Heat Transmission", 3rd Ed., McGraw-Hill, (1954).

18. E. Speyer, "Solar energy collection with evacuated tubes," J. Engr. Power, Vol. 86, p 270, (1965).

19. D. C. Beakley and G. R. Mather, " Analysis and experimental tests of high performance tubular solar collectors," Paper 32-10, ISES 1975 Solar Energy conference and Exposition, Los Angeles, (1975).

20. V. Ortabasi and W. M. Buehl, "Analysis and performance of an evacuated tubular collector," Paper 32-11, ISES 1975 Solar Energy Conference and Exposition, Los Angeles, (1975).

21. C. B. Eaton and H. A. Blum, "The use of moderate vacuum environments as a means of increasing the collection efficiencies of flat-plate solar collectors," Solar Energy, Vol. 17, No. 3, pp 151-158, (1975).

22. K. G. T. Hollands, "Honeycomb devices in flat-plate solar collectors," Solar Energy, Vol. 9, pp 159-168, (1965).

23. D. K. Edwards, "Suppression of cellular convection by lateral walls," J. Heat Transfer, Vol. 91, pp 145-152. (1969).

24. W. Charters and L. Peterson, "Free-convection suppression using honeycomb cellular materials," Solar Energy, Vol.13, No. 4, (1972).

25. K. G. T. Hollands and L. Konicek, "Experimental study of the stability of differentially heated inclined air layers," Int'l. J. Heat and Mass Transfer, Vol. 16, pp 1468-1473. (1973).

26. G. K. Batchelor, "Heat transfer by free convection across a closed cavity between vertical boundaries at different temperatures", Q. Appl. Math., Vol. 12, pp 209-218, (1954).

27. R. L. Cane et al, "Convection suppression in inclined honeycombs," Paper 32-75, ISES 1975 Solar Energy Conference and Exposition, Los Angeles, (1975).

28. H. Buchberg and D. K. Edwards, "Design Considerations for solar collectors with cylindrical glass honeycombs," Solar Energy, Vol. 18, No. 3, pp 193-209, (1976).